LOI to JLab PAC31

Study of Hypernuclei by Pionic Decay at JLab

A. Margaryan[1], O. Hashimoto[2], S. Majewski[3], L. Tang[3]

[1] *Yerevan Physics Institute, 375036 Yerevan, Armenia*
[2] *Tohoku University, Sendai, 98-77, Japan*
[3] *Thomas Jefferson National Accelerator Facility, Newport News, VA 23606, USA*

Abstract

In this letter, we propose to investigate Λ hypernuclei for the $A \leq 15$ mass region by using pionic decay. The Project aims to determine precisely the binding energies of light hypernuclei, investigate production of exotic hypernuclei, and study impurity nuclear physics and the medium effect of baryons.

These investigations will fully utilize the unique parameters (high intensity, small emittance and fine beam bunch time structure) of the CW electron beams at Jefferson Laboratory, and are enabled by (1) the use of high-resolution kaon spectrometer (HKS) in Hall C, (2) the development of a high-resolution magnetic spectrometer for hypernuclear decayed pions ($H\pi S$), (3) the development of a Cherenkov picosecond timing technique based on the recently proposed RF picosecond phototubes.

Light hypernuclei ground state binding energy measurements must have a precision about 100 keV. Their average values will be determined with a precision better than 10 keV.

We propose to start with HKS and $H\pi S$ with a conventional timing technique and carry out a pilot experiment by using ^{12}C, ^{7}Li and ^{4}He targets and simultaneously develop the RF Cherenkov picosecond timing technique for the next step hypernuclear studies at Jefferson Laboratory.

1. Introduction

The binding energies of the Λ particle in the nuclear ground state give one of the basic pieces of information on the Λ-nucleus interaction. Most of the observed hypernuclear decays take place from the ground states, because the electromagnetic interactions or Auger neutron emission process are generally faster than the weak decay of the Λ particle. The binding energy of Λ in the ground state is defined by:

$B_\Lambda(g.s.) = M_{core} + M_\Lambda - M_{HY}$.

The mass M_{core} is merely the mass of the nucleus that is left in the ground state after the Λ particle is removed. The binding energies, B_Λ, have been measured in emulsion for a wide range of light ($3 \le A \le 15$) hypernuclei [1]. These have been made exclusively from π^--mesonic decays. The precise values of the binding energies of Λ in the few-baryon systems provide filters through which one can look at particular aspects of the YN interaction, and one of the primary goals in hypernuclear physics is to extract information about YN interactions through precise calculations of few-body systems such as ${}^{3}_{\Lambda}H, {}^{4}_{\Lambda}H, and\ {}^{4}_{\Lambda}He$. The existing situation can be summarized by the help of words of R. Dalitz [2]:

" ${}^{3}_{\Lambda}H$ was well known very early and has been studied a great deal. Its B_Λ value is quite small and difficult to measure. It was the first hypernucleus to be considered a "Λ halo". The value of 0.13 ± 0.05 MeV by Don Devis [1] quoted above was from emulsion studies. From HeBC studies, Keyes et al. [3] have given 0.25 ± 0.31 MeV for all events ($^3He\pi^-$) but got -0.07 ± 0.27 when they added in all other π^- modes, which is not reassuring. For $R_3 = n(^3He\pi^-)/n(^3H\pi^- \to all\pi^- \text{mod}es)$ they give $R_3 = 0.36 \pm 0.07$, and consider this to correspond to $0.11^{+0.06}_{-0.03}$ MeV for its B_Λ value. I feel that we are far from seeing the end of this road. A good deal of theoretical work on this 3-body system would still be well justified."

We propose a new experiment for precise measurement of binding energies, B_Λ, for a light ($A \le 15$) mass range of hypernuclei at CEBAF, by using again π^--mesonic decays. The expected results will provide binding energies B_Λ with a precision of about or better than 100 keV, which is 5-10 times better than in the case of emulsion. Average values of the B_Λ will be determined within an error of about 10 keV or better.

These investigations will fully utilize the unique parameters of the CEBAF electron beam and RF system and are enabled by (1) the use of HKS in Hall C, (2) the precise magnetic spectrometer for hypernuclear decayed pions (HπS), and (3) the development of an RF Cherenkov picosecond timing detector, based on recently proposed radio frequency picosecond phototubes (RFPP) [4], for separation of delayed pions from prompt ones. The combination of the last two ingredients with the CEBAF electron beam results in a high-precision and a highly sensitive unique table-top experimental setup for hypernuclear studies, and can be used not only of B_Λ precise measurement, but also for investigations of exotic hypernuclei toward to neutron and proton drip-lines, for study of π^-, π^+ decays of hypernuclei, impurity nuclear physics, and the medium effect of baryons.

We define the project with four phases as follows:

1. Phase 1: Activities devoted to the manufacturing of the RFPP.
2. Phase 2: Pilot experiment at Hall C by using HKS and HπS, e.g. modified HES with the regular timing technique.
3. Phase 3: Development, construction and test of RF Cherenkov picosecond detectors based on the RFPP.
4. Phase 4: Experiments at JLab using only HπS with the RF Cherenkov picosecond timing technique.

Phase 1-2 can be started simultaneously. Experience gained with the Pilot experiment can be used to fix future realistic hypernuclear physics program at TJNAF with the RF timing technique.

2. Physics subjects

The physics subjects which can be pursued by precision hypernuclear spectroscopy are enlightening in particular in the current Projects [5, 6] (see also [7], [8], [9], [10], [11], [12]). The physics subjects which can be studied by precise decay pion spectroscopy can be summarized as:

1) YN interactions,
2) Study of exotic hypernuclei,
3) Impurity nuclear physics, and
4) Medium effect of baryons- B(M1) measurement.

2.1 YN interaction

From precise hypernuclear ground state binding energies and detailed hypernuclear low level structure, we can establish the ΛN spin-dependent (spin-spin, spin-orbit, and tensor forces) interaction strengths, and then investigate $\Sigma N - \Lambda N$ coupling force, and charge symmetry breaking. Experimental information on these characteristics of the ΛN interaction plays an essential role to discriminate and improve baryon-baryon interaction models, not only those based on the meson-exchange picture but also those including quark-gluon degree of freedom, toward unified understanding of the baryon-baryon interactions. In addition, understanding of the YN and YY interactions is necessary to describe high density nuclear matter containing hyperons. The binding energies of light hypernuclei are the most valuable experimental information for checking different models of YN interaction. In the Table 1 taken from reference [12] lists the results of the Λ separation energies obtained as a result of ab initio calculations using YN interactions with an explicit Σ admixture. It is demonstrated that for future theoretical developments more precise experimental measurements for binding energies are needed.

Table 1: Λ separation energies, given in units of MeV, of A = 3-5 Λ hypernuclei for different YN interactions.

YN	$B_\Lambda({}^{3}_{\Lambda}H)$	$B_\Lambda({}^{4}_{\Lambda}H)$	$B_\Lambda({}^{4}_{\Lambda}H^{*})$	$B_\Lambda({}^{4}_{\Lambda}He)$	$B_\Lambda({}^{4}_{\Lambda}He^{*})$	$B_\Lambda({}^{5}_{\Lambda}He)$
SC97d(S)	0.01	1.67	1.2	1.62	1.17	3.17
SC97e(S)	0.10	2.06	0.92	2.02	0.90	2.75
SC97f(S)	0.18	2.16	0.63	2.11	0.62	2.10
SC89(S)	0.37	2.55	Unbound	2.47	Unbound	0.35
Experiment	0.13 ± 0.05	2.04 ± 0.04	1.00 ± 0.04	2.39 ± 0.03	1.24 ± 0.04	3.12 ± 0.02

In addition, the π^- decay can be used to obtain spectroscopic information on hypernuclear structure, due to the selective character and sensitive shell-structure dependence [13], [14].

2.2 Study of exotic hypernuclei

There is currently in the nuclear physics community a strong interest in the study of nuclei very far from the valley of stability. It would allow one to apprehend the behavior of nuclear matter under extreme conditions. Hypernuclei can be even better candidates than ordinary nuclei to study nuclear matter with extreme N/Z ratios because more extended mass distributions are expected than in ordinary nuclei thanks to the glue-like role of the Λ, and its effect on neutron halo [15]. In Table 2 (see below) we see many particle stable hypernuclei with unstable cores: ${}^{6}_{\Lambda}He$, ${}^{7}_{\Lambda}Be$, ${}^{8}_{\Lambda}He$, ${}^{9}_{\Lambda}Be$. Other hypernuclei with neutron excess may exit: e.g. ${}^{6}_{\Lambda}H$, ${}^{7}_{\Lambda}H$, ${}^{8}_{\Lambda}H$, ${}^{10}_{\Lambda}He$, ${}^{11}_{\Lambda}Li$ (see also [16], [17]). These hypernuclei and other exotic hypernuclei with neutron and proton excess are expected to be photoproduced indirectly (see below) on heavy targets and their two-body pionic decays can be detected by $H\pi S$.

2.3 Impurity nuclear physics

Since hyperons are free from the Pauli effect and feel nuclear forces different from those nucleons do in a nucleus, a hyperon introduced in a nucleus may give rise to various changes of the nuclear structure, such as changes of the size and the shape, change of the cluster structure, emergence of new symmetries, change of collective motions, etc. A beautiful example of how we may modify a nucleus by adding to it a distinguishable baryon in a well defined state is given by the experiment on γ spectroscopy of ${}^{7}_{\Lambda}Li$. ${}^{7}_{\Lambda}Li$ is produced by means of the reaction $\pi^+ + {}^7Li \rightarrow {}^{7}_{\Lambda}Li + K^+$ at 1.05 GeV/c using the SKS spectrometer at KEK. ${}^{7}_{\Lambda}Li$ may be formed in the ground or low lying excited states. When a Λ in a 1s orbit is added to a loosely bound nucleus such as ${}^6Li$, the nucleus is expected to shrink into a more compact system due to the attractive force between Λ and nucleons ("glue-like" role of the Λ) which results from the property of the Λ of being free from the Pauli blocking in a nucleus. This effect can be verified from the E2 transition probability B(E2), which contains information of the nuclear size. The E2 ($5/2^+ \rightarrow 1/2^+$) transition of ${}^{7}_{\Lambda}Li$ is essentially the E2 ($3^+ \rightarrow 1^+$) transition of the core nucleus ${}^6Li$, but the existence of a Λ in the 1s orbit is expected to shrink the ${}^6Li$ core. Experimentally, B(E2) is derived from the lifetime of the $5/2^+$ state. The expected lifetime (~10^{-11} sec) is of the same order of the stopping time of the recoil ${}^{7}_{\Lambda}Li$ in lithium in the case of the (π^+, K^+) reaction at 1.05 GeV/c and was derived to be $5.8^{+0.9}_{-0.7} \pm 0.7$ ps with the Doppler shift attenuation method (DSAM). B(E2) was then derived to be $3.6 \pm 0.5^{+0.5}_{-0.4}$ e^2fm^4. This result, compared with the $B(E2) = 10.9 \pm 0.9$ e^2fm^4 of the core nucleus ${}^6Li(3^+ \rightarrow 1^+)$, indicates shrinkage of the ${}^{7}_{\Lambda}Li$ size from ${}^6Li$ by about 20% [18, 19].

The Doppler shift attenuation method can be applied to measure lifetimes of the $10^{-12} - 10^{-11}$ sec region, as in the B(E2) measurement of ${}^{7}_{\Lambda}Li$. For the M1 transition with energy less than 0.1 MeV and E2 transition with energy around 1 MeV the expected lifetimes are too long ($\sim 10^{-10}$ sec) for DSAM and the γ transition competes with weak decay. For this case a new "γ – weak coincidence method" has been proposed [20].

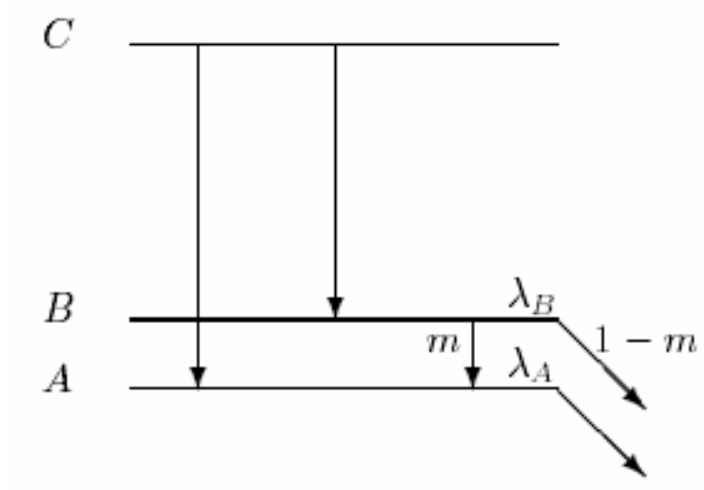

Figure 1: Method of B(E2) and B(M1) measurement from coincidence events of γ-ray and weak-decay particles.

This method allows to determine the transition probability from the total decay rate (λ_B) of the upper state B (Fig. 1) and branching ratio (m) of the γ decay. The lifetime of B is directly measured from the time difference of hypernuclear production and emission of weak-decay particles (p and π^-). If γ transitions to populate B from upper states (C) are much faster than the

total decay rate of B(λ_B), as is usually the case for a small ground doublet spacing, the time spectrum of weak decay particles measured in coincidence with the $B \to A\,\gamma$ ray is expressed as:

$$P^{B\to A}(t) = \frac{\lambda_A \lambda_B}{\lambda_A - \lambda_B} m N_B (e^{-\lambda_A t} - e^{-\lambda_B t}),$$

where λ_A denotes the decay rate of A and N_B denotes the initial population of the state B (including $C \to B$). From this growth-decay function, λ_A and λ_B can be determined.

When the $B \to A$ transition is much slower than the weak decay, λ_B is determined from the time spectrum of weak decay particles in coincidence with $C \to B\,\gamma$ rays, which is expressed as:

$$P^{C\to B}(t) = \lambda_B N_B^{C\to B}[(1 - m\frac{\lambda_B}{\lambda_B - \lambda_A})e^{-\lambda_B t} + m\frac{\lambda_A}{\lambda_B - \lambda_A}e^{-\lambda_A t}].$$

Here, $N_B^{C\to B}$ is the population of B via the fast $C \to B$ transition. In general by measuring both $P^{B\to A}(t)$ and $P^{C\to B}(t)$, and fitting them to the equations above, λ_B can be determined precisely in a wide range. The branching ratio m of the $B \to A$ transition is measured from the γ-ray yield of $B \to A$ transition in coincidence with the $C \to B$ transition.

In our case the high momentum resolution and high time resolution of $H\pi S$ allow us to separate pionic decays from the A and B states (see e.g. Fig. 2) and to measure precisely the weak decay time spectra $P^{B\to weak}(t)$ and $P^{A\to weak}(t)$ separately. The time spectrum of weak-decay pions from the B state is:

$$P^{B\to weak}(t) = (1-m)\lambda_B N_B e^{-\lambda_B t}.$$

The time spectrum of weak-decay pions from A state is:

$$P^{A\to weak}(t) = P^{B\to A}(t) + \lambda_A N_A e^{-\lambda_A t},$$

where N_A denotes the initial population of the state A (including $C \to A$). By measuring both of $P^{B\to weak}(t)$ and $P^{A\to weak}(t)$ and fitting them together to the equations above λ_A, λ_B and m can be determined precisely. In general it is assumed that weak decay rates of A and B states are the same, $\lambda_A = \lambda_W$, $\frac{1}{\lambda_B} = \frac{1}{\lambda_W} + \frac{1}{\lambda_\gamma}$ and $m = \frac{\Gamma_\gamma}{\Gamma_\gamma + \Gamma_w} = \frac{\lambda_w}{\lambda_\gamma + \lambda_w}$.

We call it the "tagged weak π^- decay method". It can be used for investigation of E2 or M1 transitions with lifetimes in the range of about 50–400 ps.

2.4 Medium effect of baryons – B(M1) measurement

Using hyperons free from the Pauli effect, we can investigate possible modification of baryons in nuclear matter through magnetic moments of hyperons in a nucleus. Magnetic moments of baryons can be well described by the picture of constituent quark models in which each constituent quark has a magnetic moment of a Dirac particle having a constituent quark mass. If the mass (or the size) of a baryon is changed in a nucleus by possible partial restoration of chiral symmetry, the magnetic moment of the baryon may be changed in a nucleus. A Λ particle in a hypernucleus is the best probe to see whether such an effect really exists or not. Here we propose to derive a g-factor of Λ in the nucleus from a probability (B(M1) value) of a spin-flip M1 transition between hypernuclear spin-doublet states. In the weak coupling limit between a Λ and a core nucleus, the B(M1) is expressed as [21]

$$B(M1) \propto \left|\left\langle \phi_{lo} \middle| \mu^z \middle| \phi_{up} \right\rangle\right|^2 = \left|\left\langle \phi_{lo} \middle| g_N J_N^z + g_\Lambda J_\Lambda^z \middle| \phi_{up} \right\rangle\right|^2 \propto (g_N - g_\Lambda)^2$$

where g_N and g_Λ denote effective g-factors of the core nucleus and the Λ, and J_N^z and J_Λ^z denote their spin operators, respectively. Here the space components of the wavefunctions of the lower and upper states of the doublet (ϕ_{lo}, ϕ_{up}) are assumed to be identical.

Transition probabilities such as B(M1) are derived from lifetimes of low lying excited states, using the "Doppler shift attenuation method" or "γ-weak coincidence method" [7], [8], [20].

We propose to use the "tagged weak π^- decay method" described above. Here we consider the case of ${}^{12}_{\Lambda}C$ for example. The ground-state doublet spacing of ${}^{12}_{\Lambda}C$ is predicted to be 0.071 MeV [22]. The upper and ground states in our case can be separated by the decay π^- momentum spectra. This is demonstrated in Fig. 2, where the simulated spectra with 10^5 pions (99.0% quasi-free, 0.5% 91.39 and 0.5% 91.461 MeV/c monochromatic lines) produced in the 4.8 mg/cm^2 carbon target and measured in the $H\pi S$ with precision $\sigma = 10^{-4}$, are presented (for details of simulation see below).

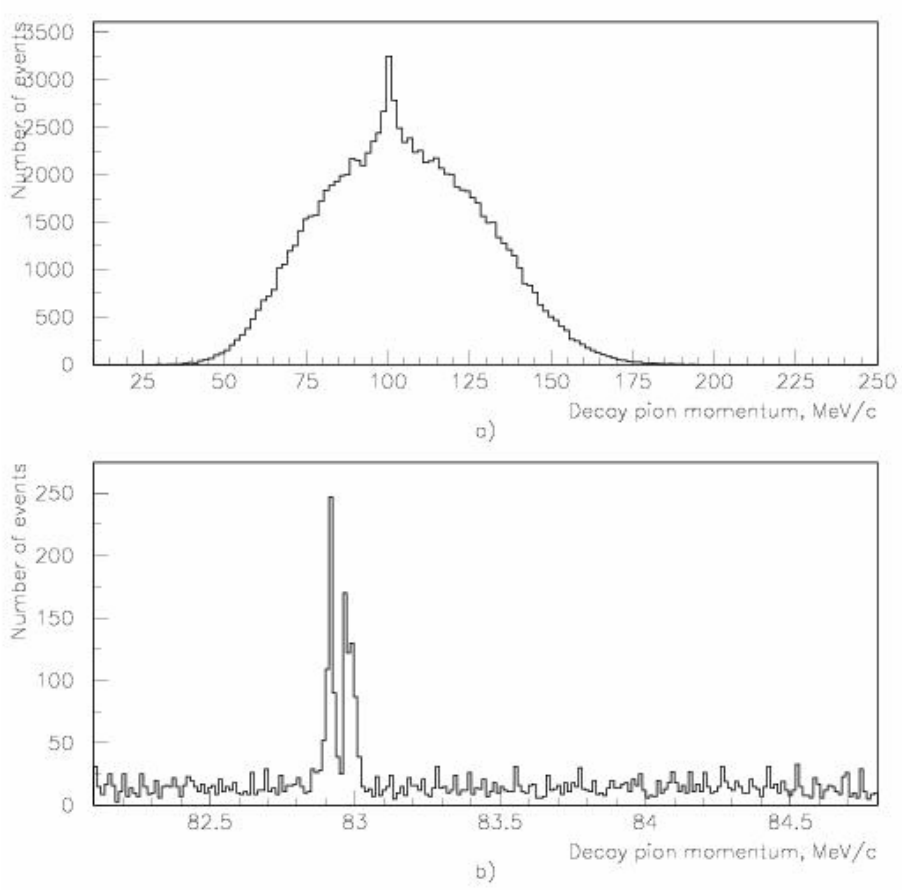

Figure 2: Simulated spectrum of the decayed pions from quasi free produced Λ particles (a) and from ${}^{12}_{\Lambda}C \rightarrow {}^{12}N^* + \pi^-$ decay [21] (b) (99.0% quasi-free, 0.5% 82.929 and 0.5% 83.0 MeV/c monochromatic lines). Target thickness is 4.8 mg/cm^2, precision of the $H\pi S$ is $\sigma = 10^{-4}$.

The B(M1) of this transition is predicted to be 0.44 μ_N^2 [20, 21], which corresponds to a decay rate of $(360\ \text{ps})^{-1}$ for 0.071 MeV. By assuming that the weak decay rate of the upper (2^-) state is the same as that of the ground (1^-) state, $(228\ \text{ps})^{-1}$, we estimate the branching ratio of the γ transition to be $m = 0.39$. Due to this the lifetime of the upper state is become 140 ps and can be easily measured by $H\pi S$, the time resolution of which with the RF Cherenkov picosecond timing technique is expected to be about 30 ps FWHM. For 1000 such kind of pionic decays, the expected life time of the upper state (140 ps) and the splitting energy (71 keV) can be determined

with about few ps and few keV precisions. Determination of the splitting energy can be used to check the YN interaction, life-time measurement to check the B(M1) modification.

3. Previous experiments and current projects

Λ hyperon separation energies B_Λ have been measured in emulsion for a wide range of light ($3 \le A \le 15$) hypernuclei. The kinematical analysis of decay fragments in nuclear emulsion in the past was the best method for determining the binding energy of the Λ particle in the hypernucleus. These have been made exclusively from π^- -mesonic decays. Identification was established if one, and only one, energy and momentum balance was obtained after permuting all possible identities of the nuclear decay particles. The emulsion data on B_Λ values, culled from some 36000 π^- -mesonic decaying hypernuclei produced by stopping K^- mesons [1, 23], are summarized in Table 2. This compilation included 4042 uniquely identified events.

Table 2: Λ binding energies B_Λ (MeV) of light hypernuclei measured in emulsion. In addition to the quoted statistical errors, there are systematic errors of about 0.04 MeV. Calculated corresponding decay pion momentum and number of observed events are presented as well.

Hypernuclide	B_Λ (MeV)	Two body π^- decay momentum (MeV/c)	Number of events
${}^{3}_{\Lambda}H$	0.13 ± 0.05	114.3	204
${}^{4}_{\Lambda}H$	2.04 ± 0.04	132.9	155
${}^{4}_{\Lambda}He$	2.39 ± 0.03	97.97	279
${}^{5}_{\Lambda}He$	3.12 ± 0.02	99.14	1784
${}^{6}_{\Lambda}He$	4.18 ± 0.1	108.4	31
${}^{7}_{\Lambda}He$	Not averaged 5.44-expected	115.1 (expected)	16
${}^{7}_{\Lambda}Li$	5.58 ± 0.03	107.9	226
${}^{7}_{\Lambda}Be$	5.16 ± 0.08	95.8	35
${}^{8}_{\Lambda}He$	7.16 ± 0.7	116.3	6
${}^{8}_{\Lambda}Li$	6.80 ± 0.03	124.1	787
${}^{8}_{\Lambda}Be$	6.84 ± 0.05	97.17	68
${}^{9}_{\Lambda}Li$	8.53 ± 0.15	121.1	8
${}^{9}_{\Lambda}Be$	6.71 ± 0.04	95.96	222
${}^{9}_{\Lambda}B$	8.29 ± 0.18	96.72	4
${}^{10}_{\Lambda}Be$	9.11 ± 0.22	104.3	1
${}^{10}_{\Lambda}B$	8.89 ± 0.12	100.5	10
${}^{11}_{\Lambda}B$	10.24 ± 0.05	105.9	73
${}^{12}_{\Lambda}B$	11.37 ± 0.06	115.8	87
${}^{12}_{\Lambda}C$	10.76 ± 0.19		
${}^{13}_{\Lambda}C$	11.22 ± 0.08		34
${}^{15}_{\Lambda}N$	13.59 ± 0.15		14

The results of the compilation are illustrated also in Fig. 9 giving the B_Λ distributions for all the hypernuclear species, from where it follows that the binding energy resolutions in emulsion lie in the range 0.5-1.0 MeV.

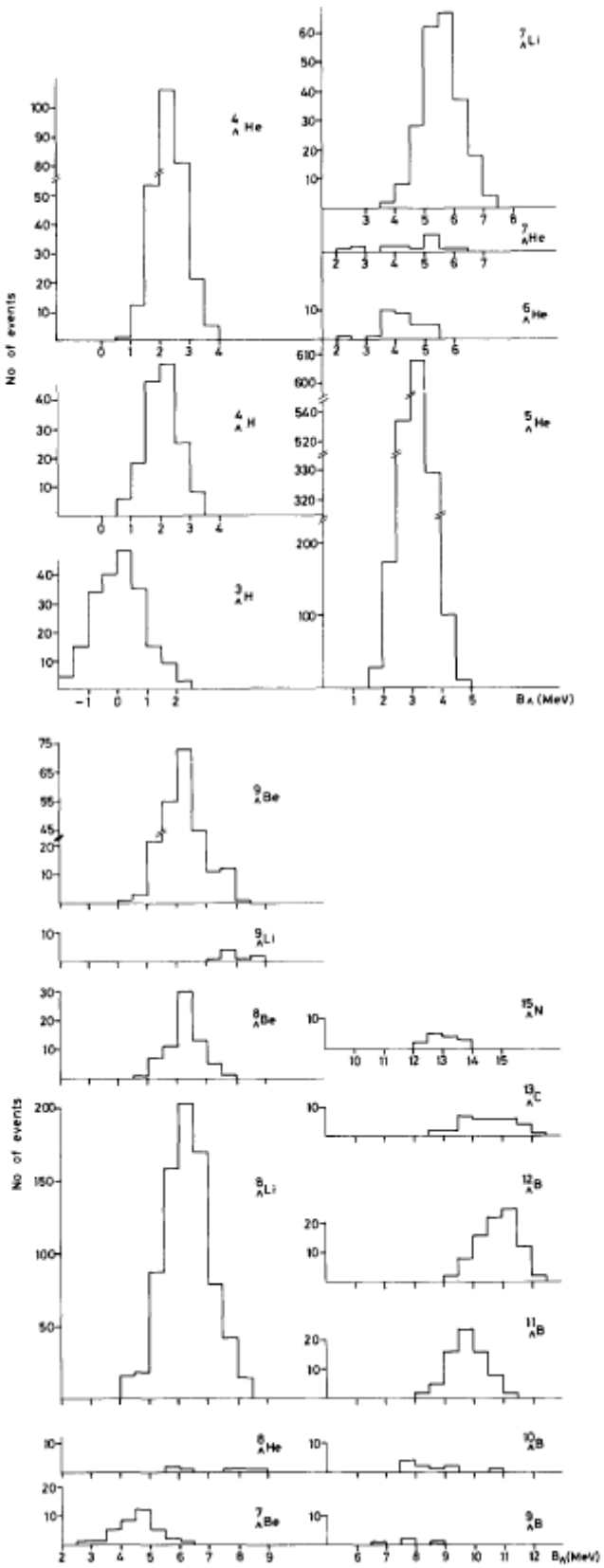

Fig. 3: Distributions of the B_Λ values for the hypernuclei of mass number $A \leq 15$. Figure is taken from reference [23].

From HeBC studies, Keyes et al. [3] have given $B_\Lambda({}^{3}_{\Lambda}H) = 0.25 \pm 0.31$ MeV for all events $({}^{3}He\pi^-)$ but got $B_\Lambda({}^{3}_{\Lambda}H) = -0.07 \pm 0.27$ MeV when they added in all other π^- modes. The Λ binding energies for some light hypernuclei were measured in the (π^+, K^+) reaction spectroscopy (see e.g. the review paper of Hashimoto and Tamura [8]) and are summarized in Table 3, where the corresponding emulsion data are presented as well.

Table 3: Λ binding energies B_Λ (MeV) of light hypernuclei measured in emulsion and in (π^+, K^+) reaction spectroscopy. In addition to quoted statistical errors, there are systematic errors of about 0.04 MeV and 0.36 MeV in emulsion and in (π^+, K^+) reaction data respectively.

Hypernuclide	B_Λ (MeV) emulsion	B_Λ (MeV) (π^+, K^+) reaction spectroscopy
${}^{7}_{\Lambda}Li$	5.58 ± 0.03	5.22 ± 0.08
${}^{9}_{\Lambda}Be$	6.71 ± 0.04	5.99 ± 0.07
${}^{10}_{\Lambda}B$	8.89 ± 0.12	8.1 ± 0.1
${}^{12}_{\Lambda}C$	10.76 ± 0.19	10.8 (fixed)
${}^{13}_{\Lambda}C$	11.69 ± 0.12	11.38 ± 0.05

The absolute mass scales of (π^+, K^+) reaction spectroscopy have been adjusted using as a reference the ${}^{12}_{\Lambda}C$ ground-state peak, whose binding energy is well determined from emulsion experiments to be 10.76 MeV. Considering the fact that the binding energies of ${}^{7}_{\Lambda}Li$ and ${}^{13}_{\Lambda}C$ agree with the emulsion data within the errors of the experiment, the difference in the cases of ${}^{9}_{\Lambda}Be$ and ${}^{10}_{\Lambda}B$ are significant even if we include systematic error (± 0.36 MeV). The reason for this disagreement is not known. These results and current theoretical investigations indicate the necessity of a new and precise measurement of the B_Λ values of light hypernuclei.

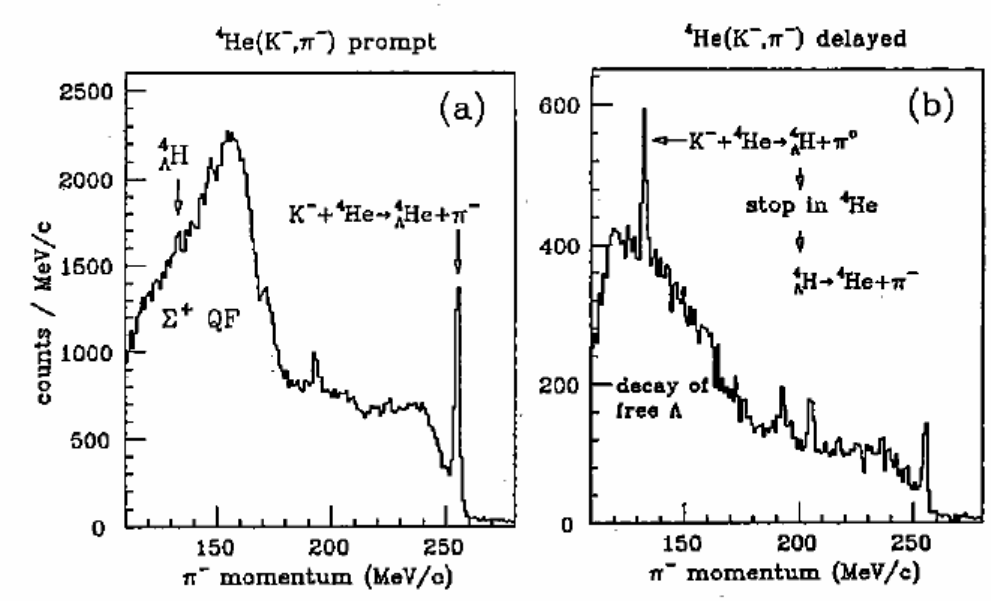

Figure 4: Time gated momentum spectra of π^- from K^- absorption at rest on ${}^{4}He$ target (from Ref. [25]. The ${}^{4}_{\Lambda}H$ peak is enhanced in the spectrum for delayed events: a) $t_{react.} \leq 0.3$ ns (prompt events); b) $0.3 \leq t_{react.} \leq 1.5$ ns (delayed events).

The hypernuclear decayed discrete π^- spectra can be measured by using a magnetic spectrometer, but in conventional fixed target experiments employing kaon beams, the need to use thick targets introduces major limitations on the achievable resolution. The momentum resolution of the Tokyo group's magnetic spectrometer e.g. was ~1 MeV [24]. However, the Tokyo group was first to detect the decayed discrete π^- mesons from ${}^{4}_{\Lambda}H$ hyperfragments as a "*delayed-particle*" in stopped K^- reactions by magnetic spectrometer (see Fig. 4 taken from Ref. [25]). This result is a clear demonstration for a new hypernuclear spectroscopy by π^- decay.

The momentum resolution of the FINUDA spectrometer [26] and the Cylindrical Detector System at J-PARC [7] is about 2 MeV in the 100 MeV/c range.

4. Production of hypernuclei

Any process which is capable of producing a Λ hyperon, may, when occurring in a nucleus, produce a hypernucleus. Two main mechanisms exist for hypernuclear formation, direct and indirect.

4.1 Direct production mechanism

Various Λ hypernuclear states can be directly populated by means of different reactions. The larger amount of data has been produced so far by means of the strangeness exchange two-body reaction: $K^- + n \to \Lambda + \pi^-$ on a neutron of a nucleus with K^- in rest and in flight. Recently, the associated production reactions $\pi^+ + n \to K^+ + \Lambda$ and $e + p \to e' + K^+ + \Lambda$ were proved to be very efficient for producing Λ -hypernuclei at KEK and at TJNAF respectively. The photon energy dependence of the elementary cross sections for the six isospin channels of kaon photoproduction is shown in Fig. 5, taken from reference [27]. The cross section for the $\gamma p \to \Lambda K^+$ reaction rises sharply at the threshold energy $E_\gamma = 0.911$ GeV and stays almost constant from 1.1 to 1.6 GeV. From the Fig. 5 it follows that in the case of the photonuclear reaction, we have three sources for K^+ mesons, with approximately equal weights. However, only the reaction $\gamma p \to \Lambda K^+$ is associated to the direct population of hypernuclear states.

The differential cross section of the $\gamma + p \to \Lambda + K^+$ reaction taken from [26] is shown in Fig. 6. From Fig. 6 it follows that at forward direction $d\sigma / d\Omega(0^\circ, \gamma + p \to \Lambda + K^+) \cong 0.35\ \mu b / sr$. The quasi-free kaon production cross section on the nucleus was assumed to scale as $Z^{0.8}$ [28] and for the differential cross section of the ${}^{12}C(\gamma, K^+)$ reaction we have about $d\sigma / d\Omega(0^\circ, \gamma + {}^{12}C \to K^+ + X) \cong 4.2 \times 0.35 = 1.47\ \mu b / sr$.

The cross sections of the hypernuclear states for the targets ${}^{7}Li$ and ${}^{12}C$ have been calculated by Motoba and Sotona for the forward produced K^+ mesons [5, 29]. They are listed in Table 4. The angular distribution of kaons in the ${}^{12}C(e, e'K^+)^{12}_{\Lambda}B$ reaction is displayed in Fig. 7. As shown in Fig. 7, the angular distribution of kaons in the ${}^{12}C(e, e'K^+)^{12}_{\Lambda}B$ reaction is forward peaked. From this distribution one can estimate that the total cross section $\sigma_t({}^{12}C(e, e'K^+)^{12}_{\Lambda}B) = \int (d\sigma / d\Omega) d\Omega \cong 31$ nb.

However, for kaons produced in the forward direction the probability of ${}^{12}_{\Lambda}B$ population or the Λ sticking probability, which is equal to the ratio of the corresponding differential cross sections, is quite high and for zero angle amounts: 0.36/1.47 = 0.24. We assume that in the angular range from 0° to 15° the quasi-free produced kaons are distributed uniformly. In such a condition the average cross section of the ${}^{12}C(e, e'K^+)^{12}_{\Lambda}B$ reaction is: $\overline{d\sigma / d\Omega(\gamma + {}^{12}C \to {}^{12}_{\Lambda}B + K^+)} \cong 170$ nb/sr and the average probability of ${}^{12}_{\Lambda}B$ population, triggered by kaons detected in the 0°-15° angular range, is equal to the ratio 0.17/1.47 ≅ 0.11.

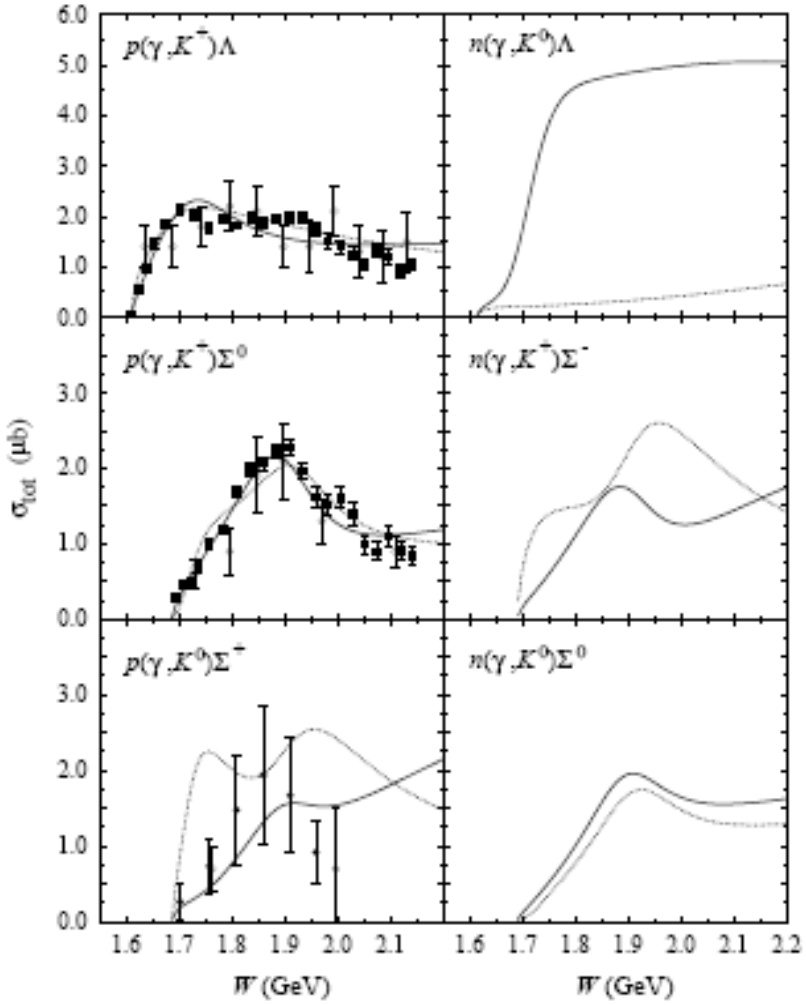

Figure 5: Total cross sections for the six isospin channels of kaon photoproduction on nucleon (from [27]).

Table 4: Cross section $d\sigma/d\Omega(\theta=0^\circ,\gamma+{}^AZ\rightarrow{}^A_\Lambda(Z-1)+K^+$ calculated by DWIA (from [5]).

Target	Hypernucleus	Hypernuclear configuration	Cross section (nb/sr)
^7Li	$^7_\Lambda He$	$s_{1/2}$	28
		$s_{1/2}$	11
		$p_{3/2}$	15
		$s_{1/2}$	52
^{12}C	$^{12}_\Lambda B$	$s_{1/2}$	112
		$p_{3/2}$	79
		$p_{1/2}$	45

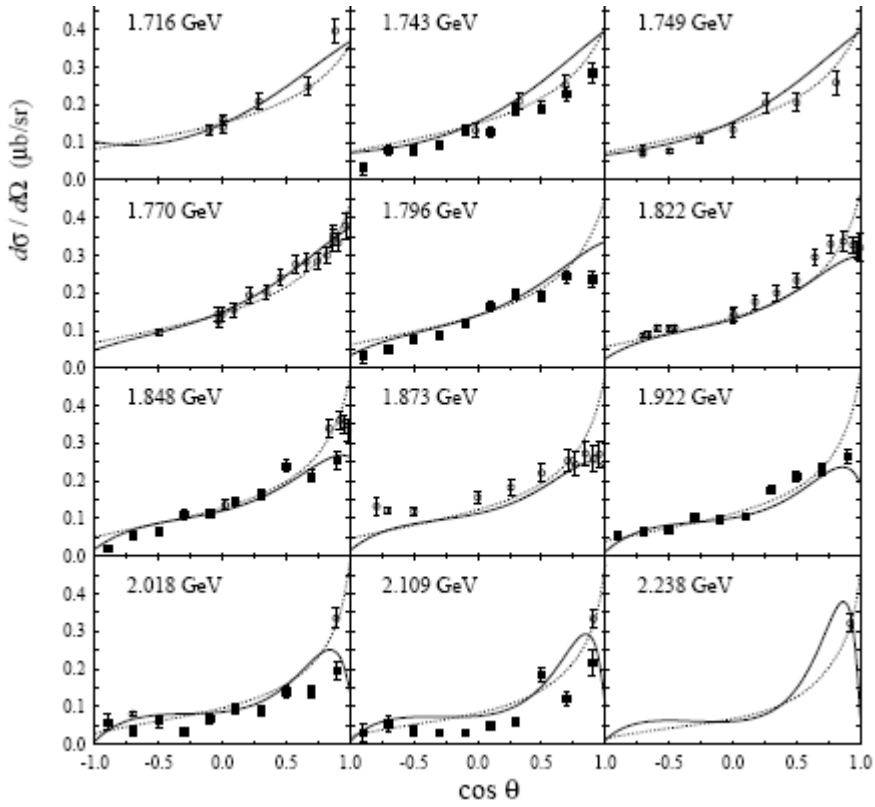

Figure 6: Differential cross section for $p(\gamma, K^+)$ channel. The total c.m. energy W is shown in every panel (for details see [27]).

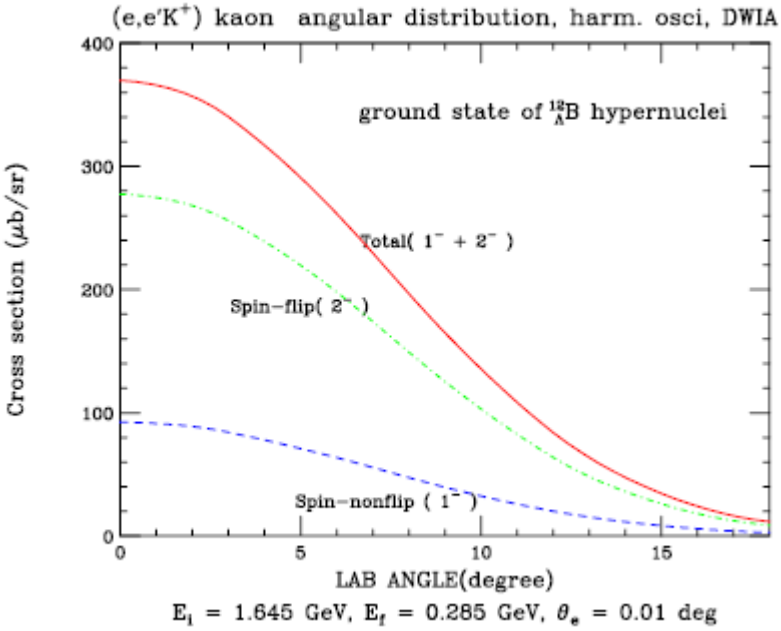

Figure 7: Angular distribution of kaon in the ${}^{12}C(e,e'K^+)^{12}_{\Lambda}B$ reaction (taken from Ref. [5]).

In future we will assume the same angular distribution for all light nuclei and 10% sticking probability for produced Λ particles, which are associated with forward produced kaons. Namely:

$$\sigma_t({}^AZ(e,e'K^+)^A_\Lambda(Z-1)) = 0.1\times Z^{0.8}\times d\sigma/d\Omega(0^\circ,\gamma+p\to\Lambda+K^+)\times\Delta\Omega\,.$$

For forward produced kaons, with $\theta_K \le 15^\circ$, $\Delta\Omega = 2\times\pi\times(\cos(0^\circ)-\cos(15^\circ)) \cong 0.2$ sr. The resulting cross sections for several targets are given in Table 6. The averaged photoproduction

cross sections for ${}^{3}_{\Lambda}H$ and ${}^{4}_{\Lambda}H$ bound states in the energy range 1-2 GeV have been estimated taking into account dedicated theoretical [30, 31] and experimental [32] investigations.

Table 6: Hypernuclear total photoproduction cross sections in nb.

Target	Hypernuclide	Cross section in nb
${}^{3}He$	${}^{3}_{\Lambda}H$	1
${}^{4}He$	${}^{4}_{\Lambda}H$	5
${}^{7}Li$	${}^{7}_{\Lambda}He$	17
${}^{9}Be$	${}^{9}_{\Lambda}Li$	25
${}^{12}C$	${}^{12}_{\Lambda}B$	31

It is assumed that about 1/3 of forward produced K^+ mesons are associated with the $\gamma + p \rightarrow \Lambda + K^+$ reaction (see Fig. 5) and therefore only about 3% of forward produced inclusive K^+ mesons are associated with direct population of hypernuclei. This will be used to estimate yields of directly produced hypernuclei in the case of coincidence experiments with forward produced kaons, e.g. with kaons detected in the HKS.

4.2 Indirect production mechanism

On the other hand, it is known from old emulsion experiments [1] that various hypernuclei, including proton or neutron rich ones, can be produced as hyperfragments by K^- induced reactions (see Table 2). Formation probabilities of ${}^{4}_{\Lambda}H$ hypernuclei in the K^- absorption at rest on ${}^{4}He, {}^{7}Li, {}^{9}Be, {}^{12}C, {}^{16}O$, and ${}^{40}Ca$ targets have been measured with the aid of the characteristic π^- (133 MeV/c) from the two-body decay of ${}^{4}_{\Lambda}H$, ${}^{4}_{\Lambda}H \rightarrow {}^{4}He + \pi^-$ at KEK [33] as well. The production rates ${}^{4}_{\Lambda}H$ obtained by the KEK group [33] and by the European K$^-$ Collaboration [1] are shown in Table 7.

Table 7: Comparison of ${}^{4}_{\Lambda}H$ production rates by stopping K$^-$ mesons.

KEK (Tokyo)		European K$^-$ Collaboration	
Target	Rate ($\times 10^{-3}$)	Target	Rate ($\times 10^{-3}$)
${}^{7}Li$	30		
${}^{9}Be$	15.7		
${}^{12}C$	10.0	C, N, O	7.3
${}^{16}O$	4.7		
${}^{40}Ca$	≤ 2.7	Ag, Br	2.4

Similarly, rates of production of ${}^{3}_{\Lambda}H$ and ${}^{5}_{\Lambda}He$ by stopping K^- mesons have been deduced [1] and are given in Table 8.

Table 8: Production rates of ${}^{3}_{\Lambda}H$ and ${}^{5}_{\Lambda}He$ measured by the European K^- collaboration.

Target	${}^{3}_{\Lambda}H$ rate $(\times 10^{-3})$	${}^{5}_{\Lambda}He$ $(\times 10^{-3})$
C, N, O	1.62	21.6
Ag, Br	0.54	1.4

It is to be noted that the ${}^{4}_{\Lambda}H/{}^{3}_{\Lambda}H$ production ratio is ≈ 5 for both light and heavy targets. The large drop in ${}^{5}_{\Lambda}He$ production in going from light to heavy targets is explained by the strong inhibition of helium emission due to the high Coulomb barrier presented by silver and bromine nuclei.

From observations of neutral hyperon emission it has been shown that the overall hypernuclear production rates by stopping K^- mesons are $8 \pm 2\%$ from C, N, O and $58 \pm 15\%$ from Ag, Br.

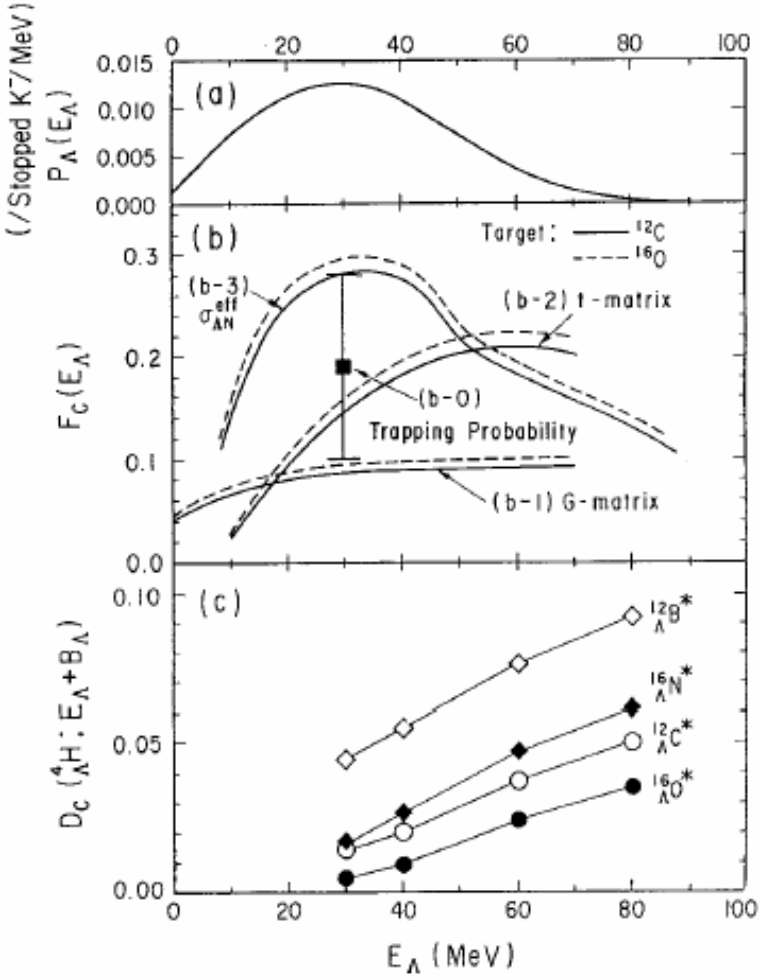

Figure 8: (a) The calculated energy distribution of Λ produced from K^- absorption at rest. (b) The formation probabilities of the Λ compound nucleus on C and O targets, $F_C(E_\Lambda)$, estimated in four different ways, from the experimental hyperon trapping probability (b-0), from the imaginary part of the Λ potential calculated by the G-matrix (b-1) and by the t-matrix (b-2), and estimated by Yazaki from the ΛN cross section with the Pauli suppression effect (b-3). (c) The fragmentation probabilities of ${}^{4}_{\Lambda}H$ from the Λ compound nucleus, $D_C({}^{4}_{\Lambda}H, E_X = E_\Lambda + B_\Lambda)$ calculated for ${}^{12}_{\Lambda}C^*, {}^{12}_{\Lambda}B^*, {}^{16}_{\Lambda}O^* and {}^{16}_{\Lambda}N^*$ (taken from Ref. [34]).

The two body reactions for K^- absorption at rest, which produce strangeness (which finally results in a Λ hyperon) in the nucleus, are listed in Table 9.

Table 9: Two body reactions that for K^- absorption at rest produce strangeness (Λ hyperon).

$K^- + p \rightarrow \Lambda + \pi^0$	$K^- + n \rightarrow \Lambda + \pi^-$
$K^- + p \rightarrow \Sigma^- + \pi^+$	$K^- + n \rightarrow \Sigma^- + \pi^0$
$K^- + p \rightarrow \Sigma^0 + \pi^0$	$K^- + n \rightarrow \Sigma^0 + \pi^-$
$K^- + p \rightarrow \Sigma^+ + \pi^-$	

The observed formation probabilities of hyperfragments per stopped K^- could be explained by a model in which a quasi-free produced Λ is trapped in the nucleus and forms a "Λ compound nucleus", which may decay into a hyperfragment such as ${}^{4}_{\Lambda}H$. In this model, which was proposed by Tamura et al. [34], the ${}^{4}_{\Lambda}H$ formation probabilities per produced Λ can be expressed in terms of three physical factors as:

$$P({}^{4}_{\Lambda}H) = \int P_{\Lambda}(E_{\Lambda}) F_C(E_{\Lambda}) D_C({}^{4}_{\Lambda}H, E_X) dE_{\Lambda} \ .$$

Where, $P({}^{4}_{\Lambda}H)$ represents the energy distribution of produced Λ. $F_C(E_{\Lambda})$ stands for the formation probability of a Λ compound nucleus, when a Λ with a kinetic energy E_{Λ} is produced. $D_C({}^{4}_{\Lambda}H, E_X)$ is the probability of forming ${}^{4}_{\Lambda}H$ from the Λ compound nucleus with excitation energy E_X. The calculated values in the case of stopped K^- are shown in the Fig. 8. According to this model, formation probabilities of ${}^{4}_{\Lambda}H$ hyperfragments are higher for higher energy Λ hyperons. The momentum transferred to the produced Λ hyperon with K^- at rest is about 250 MeV/c. Therefore one can expect that about the same or even more abundant hyperfragments must be produced in the electromagnetic production of a Λ hyperon, where the momentum transfer to the Λ hyperon is in the range of 250-450 MeV/c for photons in the energy range of 1-2 GeV.

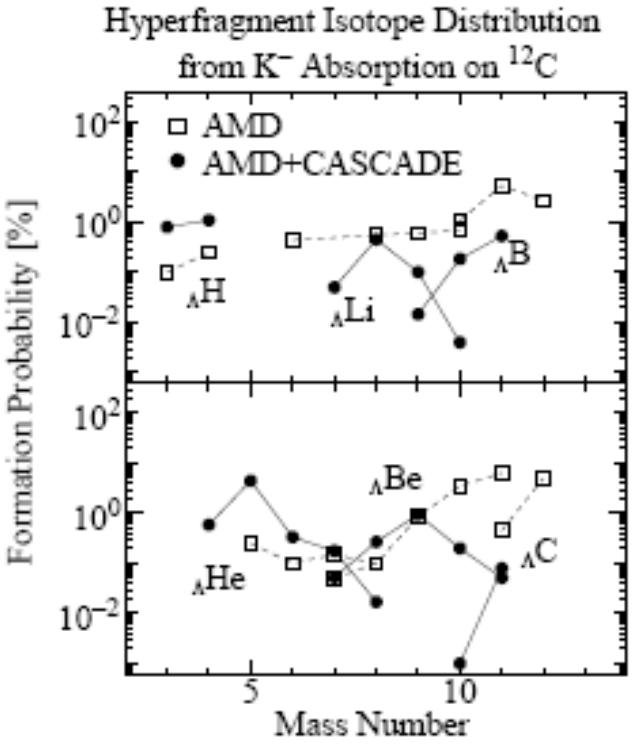

Figure 9: Hyperfragment isotope distribution from K^- absorption at rest on ^{12}C (from [35]). Boxes are the results of AMD calculation and black circles are the results after the multi-step statistical decay calculation.

The formation probability of ${}^{4}_{\Lambda}H$ from K^- absorption at rest on light nuclear targets was also investigated by employing antisymmetrized molecular dynamics (AMD) combined with multi-step binary statistical decay [35]. The calculated hyperfragment isotope distribution of a ^{12}C target is shown in Fig. 9. The total probability of *excited* hyperfragment formation amounts to about 29 %. Mass distribution of $A \leq 10$ hyperfragments produced in AMD is about one-third of the total yield of the hyperfragments and the rest is the contribution of hyperon compound nuclei with mass number A = 11 and 12. Calculated result shows good agreement with the data of ${}^{4}_{\Lambda}H$ formation (~ 1%).

These investigations demonstrate that as the target mass number decreases from ^{16}O, ^{12}C to ^{9}Be, the main formation mechanism varies from statistical decay, followed by dynamical fragmentation, to direct formation in the nuclear environment. As a result different excited parent hyperfragments are produced. To clarify the formation mechanism of ${}^{4}_{\Lambda}H$, it is worthwhile, following Nara [35] to examine the parent hyperfragment distribution of ${}^{4}_{\Lambda}H$ in the statistical decay. In Fig. 10, we show the parent hyperfragment distribution of ${}^{4}_{\Lambda}H$. We note from Fig. 10 that the sources of ${}^{4}_{\Lambda}H$ are dynamically produced neutron rich hyperfragments, and their mass numbers widely range from 6 to 12. This result gives a slightly different picture from the *hyperon compound nucleus* proposed in Ref. [34]. In Tamura's work, the sources of ${}^{4}_{\Lambda}H$ are limited to hyperon compound nuclei with mass number 11 and 12, and they have estimated the formation probability of ${}^{4}_{\Lambda}H$ to be about 0.24~0.67 %. In this work, although the contribution from these hyperon compound nuclei amounts to about 0.6%, it is found that hyperfragments with $A \leq 10$ make non negligible contributions to the formation rates of ${}^{4}_{\Lambda}H$ (~0.5%), and their sum becomes the total yield (~ 1 %). Thus the dynamical fragmentation or nucleon emission in the primary stage due to multi-step processes is indispensable for quantitative arguments, which means that due to this mechanism various exotic hypernuclei can be produced as hyperfragments that are impossible to produce by direct population.

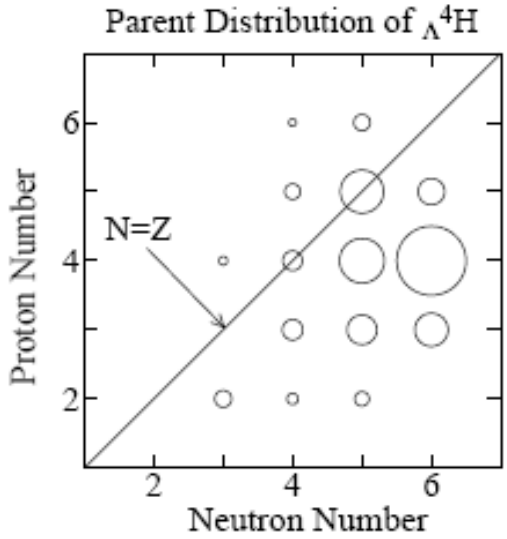

Figure 10: Parent hyperfragment distribution of ${}^{4}_{\Lambda}H$ from K^- absorption at rest on ^{12}C. The area of the circle is proportional to the probability from that hyperfragment (from [35]).

The strangeness production processes in the case of photon interactions (Table 10) are very similar to K^- induced reactions at rest. The kinematics of the K^- at rest and the photon induced two body reactions is also very similar, especially for photons in the 2 GeV energy range.

Table 10: Two body reactions that photon produce strangeness (Λ hyperon).

$\gamma + p \to \Lambda + K^+$	$\gamma + n \to \Lambda + K^0$
$\gamma + p \to \Sigma^0 + K^+$	$\gamma + n \to \Sigma^- + K^+$
$\gamma + p \to \Sigma^+ + K^0$	$\gamma + n \to \Sigma^0 + K^+$

Therefore, following to the K^- absorption at rest, the hyperfragment photoproduction cross section can be expressed as:

$$\sigma(\gamma + A \to hyperfragment + X) = A^{0.8} \times \sigma(\gamma + N \to \Lambda(\Sigma) + K) \times \varepsilon_\Lambda \times \varepsilon^i_{hyp} \ ,$$

where $\sigma(\gamma + N \to \Lambda(\Sigma) + K)$ is the strangeness phtoproduction cross section on nucleon, ε_Λ is the Λ "sticking probability", and ε^i_{hyp} is the i-th hyperfragment formation weight. The strangeness photoproduction cross section on the nucleon we define as:

$$\sigma(\gamma + N \to \Lambda(\Sigma) + K) = 0.5 \times \sigma(\gamma + p \to \Lambda(\Sigma) + K) + 0.5 \times \sigma(\gamma + n \to \Lambda(\Sigma) + K),$$

where

$$\sigma(\gamma + p \to \Lambda(\Sigma) + K) = \sigma(\gamma p \to \Lambda K^+) + \sigma(\gamma p \to \Sigma^0 K^+) + \sigma(\gamma p \to \Sigma^+ K^0),$$

$$\sigma(\gamma + n \to \Lambda(\Sigma) + K) = \sigma(\gamma n \to \Lambda K^0) + \sigma(\gamma n \to \Sigma^0 K^0) + \sigma(\gamma n \to \Sigma^- K^+).$$

Here, for crude estimation, we assume $\sigma(\gamma + N \to \Lambda(\Sigma) + K)$ = 3 μb, in the 1-2 GeV energy range (see Fig. 5), with ε_Λ = 0.1, and for ε^i_{hyp} we take the same weights which have been observed in emulsion (Table 2). For the strangeness (which finally results in the Λ particle) photoproduction cross section on ^{12}C we have:

$$\sigma(\gamma + A \to strangeness + X) = A^{0.8} \times \sigma(\gamma + N \to \Lambda(\Sigma) + K) \cong 22 \ \mu b.$$

The indirect hyperfragment photoproduction cross section on ^{12}C can be defined as:

$$\sigma(\gamma + A \to hyperfragment + X) \cong 22 \times \varepsilon_\Lambda \times \varepsilon^i_{hyp} \ \mu b.$$

The resulting cross sections for the most probable hyperfragments are shown in Table 11. In addition to hyperfragment photoproduction cross sections, relative weights of hyperfragments observed in emulsion and available experimental [1] and theoretical [13] values for π^--decay widths are listed in Table 11 as well.

Table 11: Photoproduction cross sections of light hyperfragments on ^{12}C target. In addition the relative weights and π^--decay widths are presented.

Hypernuclide	Photoproduction cross section (nb)	Relative weight	π^--decay width $\Gamma_{\pi^-}/\Gamma_\Lambda$
$^{3}_{\Lambda}H$	110	0.05	0.3
$^{4}_{\Lambda}H$	88	0.04	0.5
$^{5}_{\Lambda}He$	990	0.45	0.34
$^{7}_{\Lambda}Li$	123	0.056	0.304
$^{8}_{\Lambda}Li$	433	0.197	0.368
$^{8}_{\Lambda}Be$	37	0.017	0.149
$^{9}_{\Lambda}Be$	121	0.055	0.172
$^{10}_{\Lambda}B$	5.5	0.0025	0.215
$^{11}_{\Lambda}B$	40	0.018	0.213
$^{12}_{\Lambda}B$	48	0.01875	0.286

The Fig. 11 taken from Majling [36] shows clearly why the highly excited states of ${}^{7}_{\Lambda}He^{*}$ in which the "inner proton" is substituted by Λ ($P_s \to \Lambda_s$ transition) by means of ${}^{7}Li(\gamma, K^{+})^{7}_{\Lambda}He^{*}$ reaction are the source of hyperfragments ${}^{4}_{\Lambda}H$ and ${}^{6}_{\Lambda}H$. The thresholds for these decay channels are rather high, but large changes in the structure of these states prevent the neutron or Λ emission.

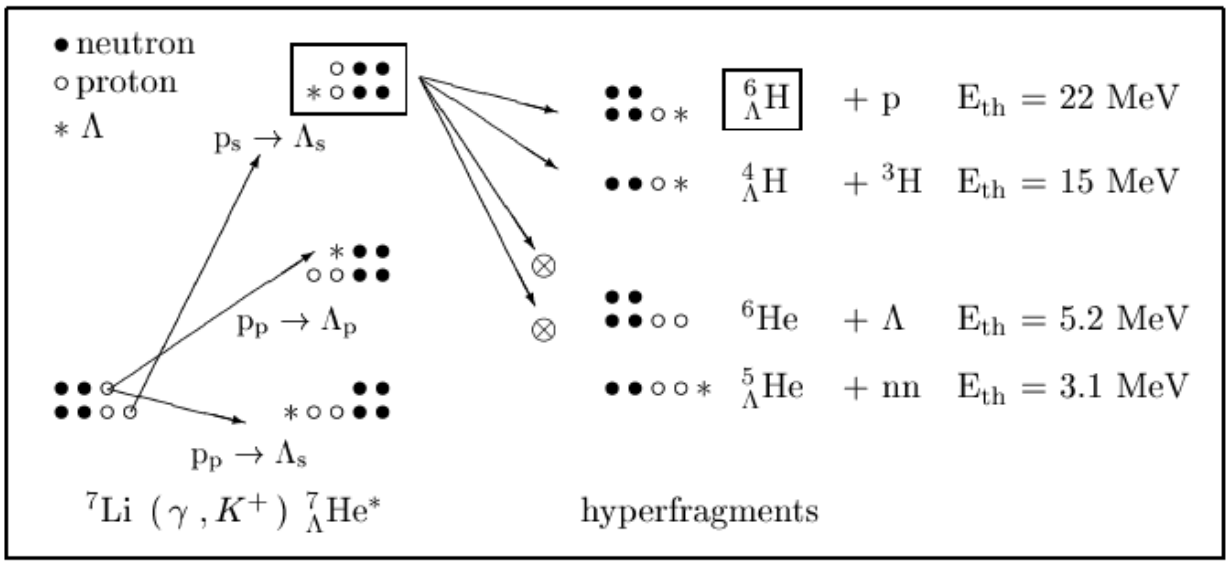

Figure 11: Different decay channels of excited ${}^{7}_{\Lambda}He^{*}$ hypernucleus.

5. Proposed Project

We propose a new project for investigation of Λ hypernuclei by using the pionic decay. The Project aims to determine precisely the binding energies of light hypernuclei, investigate production of exotic hypernuclei, and study impurity nuclear physics and the medium effect of baryons.

These investigations will fully utilize the unique parameters (high intensity, small emittance and fine beam bunch time structure) of the JLab RF driven CW electron beams, and are enabled by (1) the use of HKS in Hall C, (2) the development of a high-resolution magnetic spectrometer for hypernuclear decayed pions ($H\pi S$), (3) the development of a Cherenkov timing technique based on the recently proposed RFPP and we define the project with four phases as follows:

1. Phase 1: Activities devoted to the manufacturing of the RFPP.
2. Phase 2: Pilot experiment at Hall C by using HKS and HπS, e.g. modified HES with the regular timing technique.
3. Phase 3: Development, construction and test of RF Cherenkov detectors based on the RFPP.
4. Phase 4: Experiments at JLab using only HπS with the RF Cherenkov timing technique.

Phase 1-2 can be started simultaneously and we call this as a *First Step*. The goal of the *First Step* is to carry out pilot measurements by using existing Hall C magnetic spectrometers and their detector packages, such as HKS for forward produced kaons and a modified version of HES for decay pions, and three production targets ${}^{12}C$, ${}^{7}Li$ and ${}^{4}He$. Simultaneously, we intend to start activities devoted to the manufacturing of RFPP and developing of Cherenkov timing technique based on RFPP. *Next Step* we intend to develop dedicated magnetic spectrometer, HπS, with the RF Cherenkov timing technique and carry out wide range hypernuclear studies by decay pion. Therefore, we propose two configurations for the experiment:

(a) *First Step*: *HπS + existing HKS + existing Splitter + existing Detector Package*;

(b) *Next Step: HπS + new Detector Package based on the RF Cherenkov Timing Technique*.

We propose the experimental investigation start by using configuration (a) and simultaneously develop the RF Cherenkov timing technique for the future investigations.

6. First Step: $H\pi S$ + existing HKS + existing Splitter + existing Detector Package

6.1 Experimental setup and expected performance

The general layout of the proposed experiment is shown in Fig. 12. The incident electron beam hits the target and produces a hypernucleus. The hypernucleus is stopped in the target and decays after some 200 ps inside of the target. Decay pions have a discrete momentum lying in the range $\leq$133 MeV/c and exit the target. For the measurement of momentum of these monochromatic pions we propose to use a high-resolution pion spectrometer ($H\pi S$).

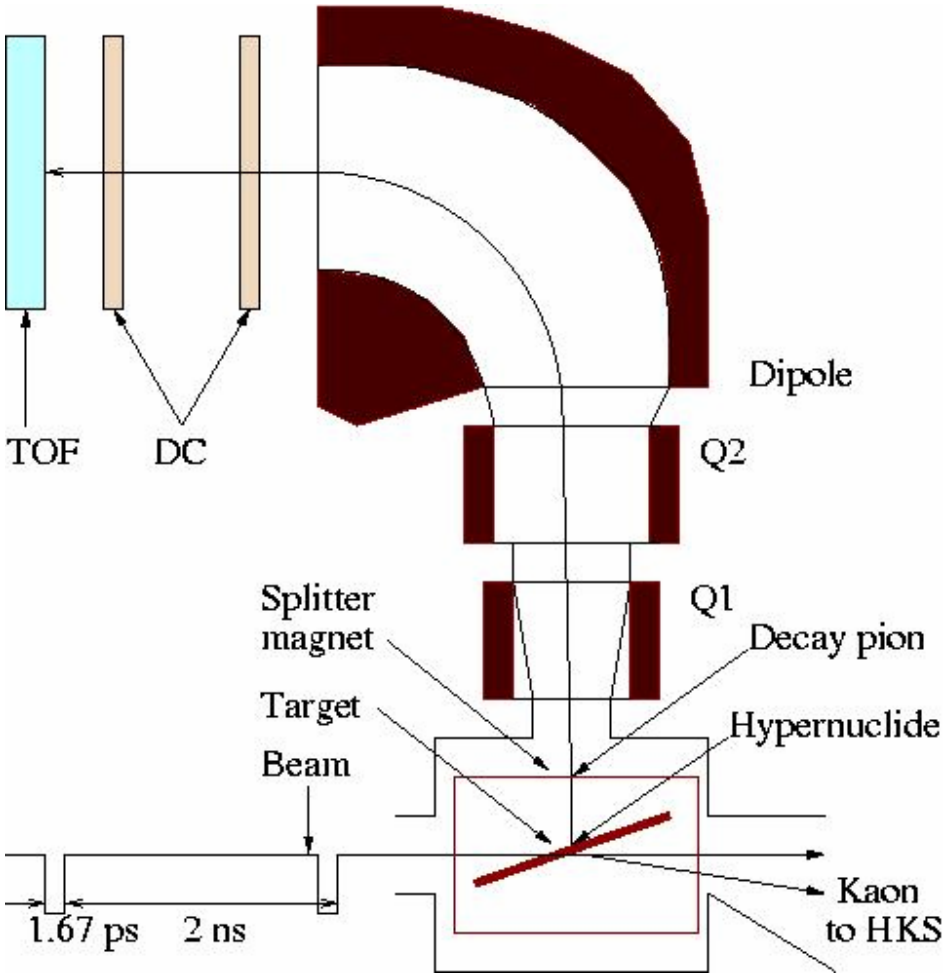

Figure 12: Plan view for the proposed experiment.

6.2 High-resolution pion spectrometer - $H\pi S$

For the measurement of decay pions in the 100 MeV/c regions, a new high resolution spectrometer with QQD configuration is proposed. It can be about 10 times smaller than the HKS or HES [5, 6]. In the first stage we can use a modified version of the HES. Table 12 shows its basic parameters.

Table 12: Parameters of the $H\pi S$ spectrometer

Configuration	Q-Q-D and horizontal bend
Central momentum	115 MeV/c
Momentum acceptance	± 20 %
Momentum resolution ($\Delta p/p$)	2×10^{-4} FWHM
Dispersion	4.7 cm/%
Pion detection angle	~90 degree relative to the incident beam
Flight path length	≤ 4 m
Solid angle	30 msr

6.3 Detector package of the $H\pi S$

The detector package of the decay pion spectrometer is basically the same as the HES detector and consists of existing tracking detectors and time-of-flight (TOF) hodoscopes.

6.4 Resolutions

The following factors contribute to the total resolution of the experiment: $H\pi S$ momentum resolution and momentum loss in the target. The energy resolution of the decay pion with velocity β_π is estimated as follows:

$$\Delta E^2 = \beta_\pi^2 \times \Delta P_\pi^2 + \Delta E_{straggling}^2,$$

where ΔP_π is the spectrometer resolution, $\Delta E_{straggling}$ is the straggling due to ionization energy loss of decay pions in the target and β_π is the velocity of the pion.

6.5 $H\pi S$ momentum resolution

The momentum resolution of the magnetic spectrometers is known to be expressed as:

$$(\tfrac{\Delta P}{P})^2 = \Delta\theta_1^2 + \Delta\theta_2^2$$

The first term is mainly determined by the optical properties of the magnetic spectrometer and spatial resolution of the detector package. The second term is determined by the multiple scattering of pions in the detector package and is proportional to $1/(P_\pi \times \beta_\pi)$. The resolution of the existing high resolution QQD magnetic spectrometers HKS or HES is about 2×10^{-4} (FWHM) in the momentum range 500-1000 MeV/c [5, 6] with a 200 μm spatial resolution detector package. The momentum resolution for the ENGE spectrometer, which used similar detector package as HES, was studied as a function of position and angular errors [5]. The results showed that with central momentum about 300 MeV/c and by using a 4th order optical matrix the momentum resolution can be about 3×10^{-4} (FWHM), if the position resolution is about 0.15 mm (r.m.s.) and the angular error is about 1mrad (r.m.s.). As follows from this simulation, the momentum resolution is about 2×10^{-4} (FWHM) due to1mrad (r.m.s.) angular error.

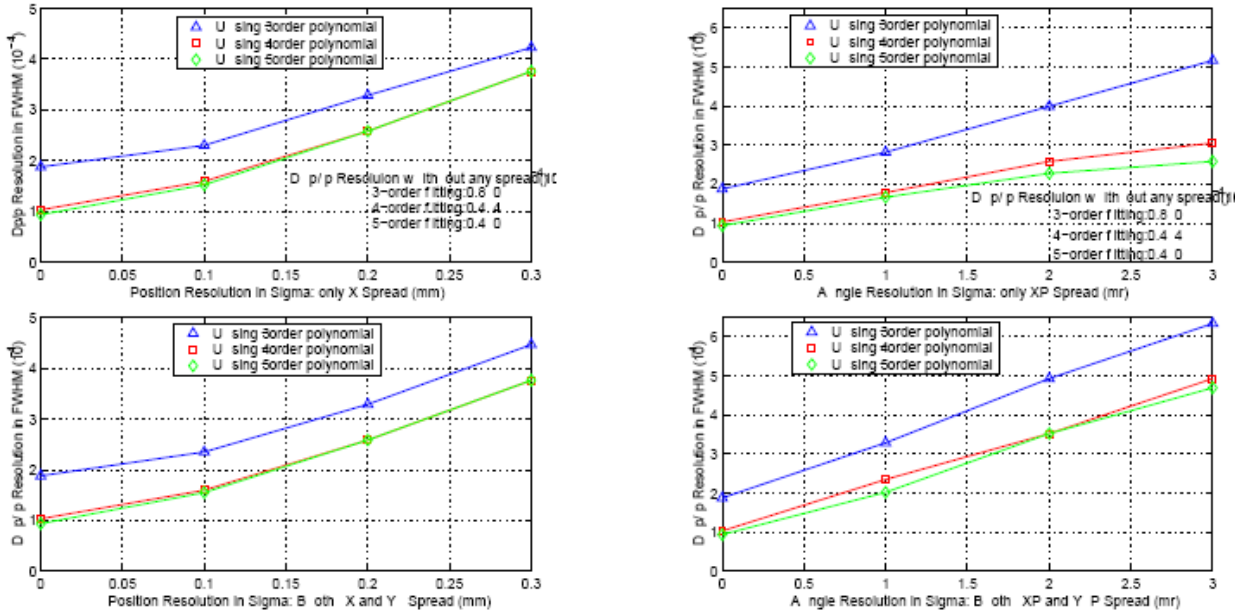

Figure 13: Momentum resolution of the Enge spectrometer for 300 MeV/c electrons (taken from reference [5], Fig. 18).

For 100 MeV/c momentum the angular error is expected to be 3 times larger, about 3 mrad, which will introduce a momentum error of about 4.8×10^{-4} (FWHM) (see Fig. 13) and the total momentum resolution will be $\frac{\Delta P}{P}=5.2\times10^{-4}$ (FWHM). In future Monte Carlo simulations we will use $\sigma=3\times10^{-4}$ for $H\pi S$ momentum resolution, which is much worse that what we can expect from the QQD magnetic spectrometer and existing detector package.

6.6 Momentum loss in the target

Due to ionization energy loss the monochromatic spectra of decayed pions is broadened. Therefore the target thickness is selected to be thin enough did not affect essentially the decay pion spectra. We have generated decay pion events and carried out a simulation study of decay pion spectra of hypernuclides by using the Monte Carlo method. The influence of the ionization energy loss has been calculated by using dedicated Monte Carlo code based on the individual collision method [37].

The dE/dx spectra of monochromatic pions ($p=115.8$ MeV/c) from ${}^{12}_{\Lambda}B\rightarrow{}^{12}C+\pi^-$ decay passing through a 24 mg/cm^2 carbon target and the broadened momentum distribution are shown in Fig. 14a and Fig. 14b respectively. Similar results obtained in the case of pions randomly distributed on a 24 mg/cm^2 carbon target are shown in Fig. 15a and Fig. 15b. From Fig. 15b it follows that the broadening due to dE/dx is about $\sigma=70$ keV/c. The decay pionic spectra produced in the 24 mg/cm^2 carbon target and measured in $H\pi S$ with precision $\sigma=3\times10^{-4}$ are shown in Fig. 15c. For the total error we have $\sigma=75$ keV/c. Similar spectra but for a 7.2 mg/cm^2 carbon target and for $\sigma=10^{-4}$ are shown in Fig. 16. For the total error in this case we have $\sigma=38$ keV/c.

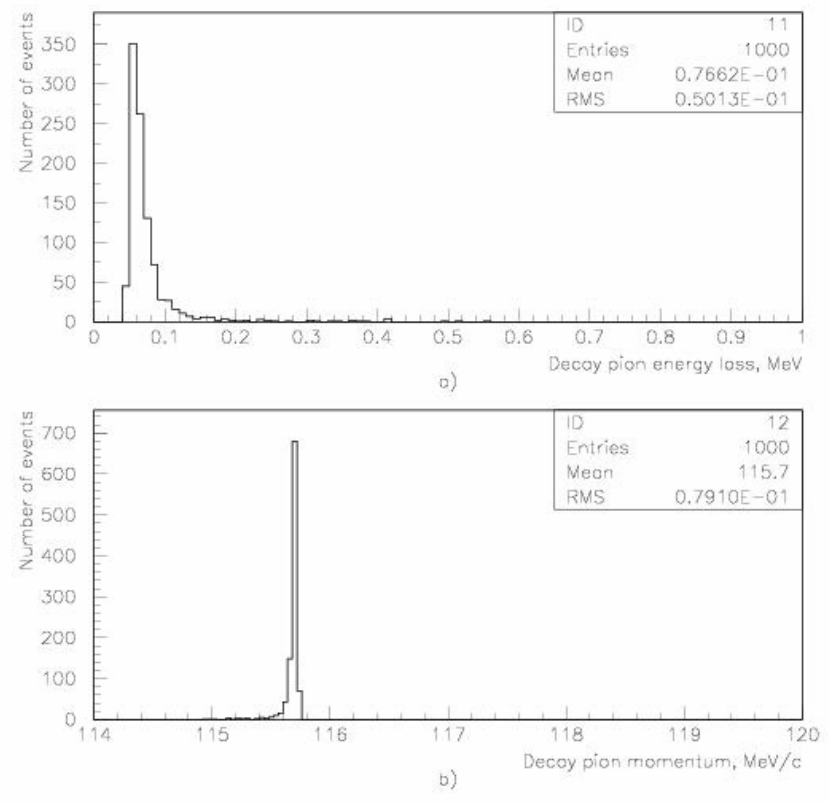

Figure 14: Simulated energy loss (a) and momentum (b) spectra of 115.8 MeV/c pions after passing through a 24 mg/cm^2 carbon target.

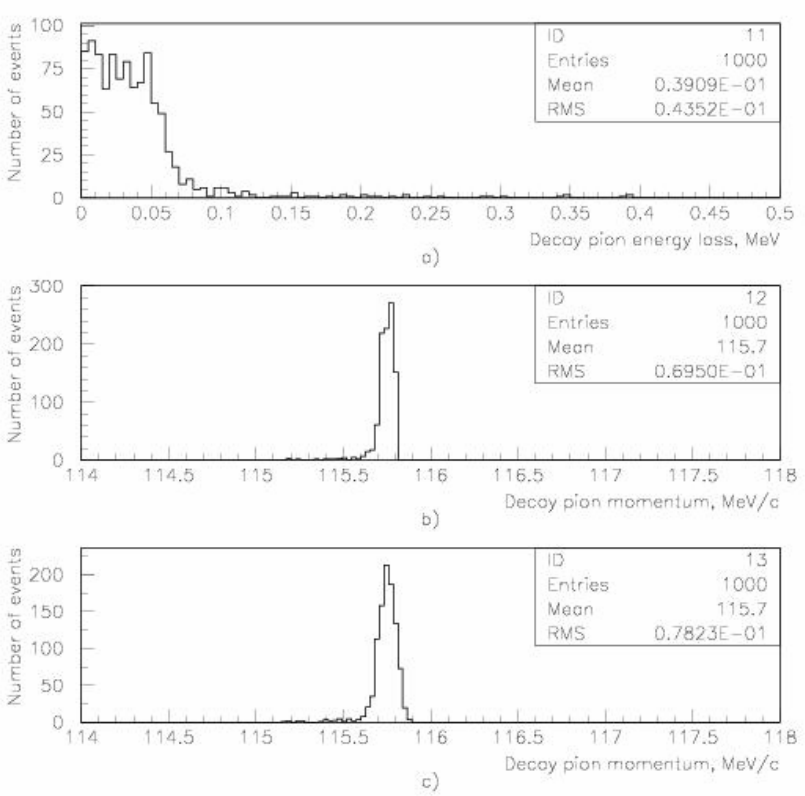

Figure 15: Simulated energy loss (a) and momentum (b) spectra for 115.8 MeV/c pions produced uniformly in the 24 mg/cm^2 carbon target; (c) is the momentum spectrum measured in the $H\pi S$ with precision $\sigma = 3\times10^{-4}$.

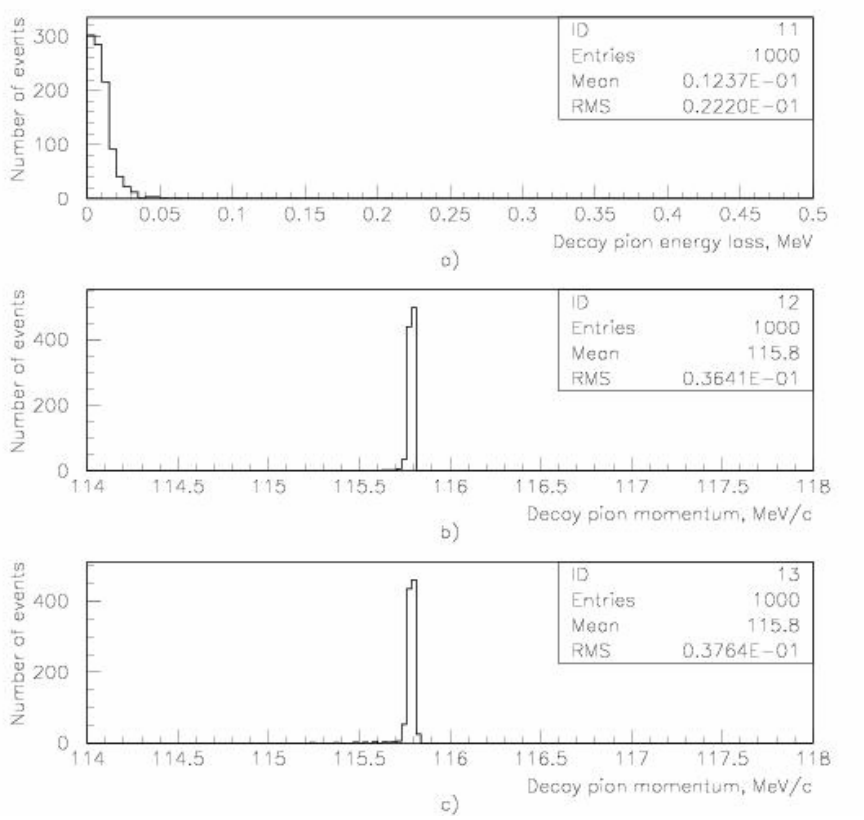

Figure 16: The same as in Fig. 4 but for the 7.2 mg /cm2 carbon target and the precision of $H\pi S$ is $\sigma = 10^{-4}$.

6.7 Summary of $H\pi S$ and Detector Package

The proposed $H\pi S$ spectrometer and detector package parameters can be summarized as:

1) Momentum resolution $\sigma \cong 3\times10^{-4}$;
2) Central momentum 115 MeV/c;
3) Momentum acceptance $\pm 20\%$;
4) Acceptance $\Delta\Omega \cong 30$ msr;
5) Time resolution $\sigma = 100$ ps;
6) Spatial resolution $\sigma = 200\,\mu m$;
7) π^- survival rate = 50% or flight path length = 4 m;
8) Vertex reconstruction $\sigma \le 1$ mm.

The electron beam raster system allows determining the reaction point on the target with precision of about 100 μm (r.m.s.). The Detector Package can provide reaction vertex reconstruction with precision of about 1 mm (r.m.s.). Time resolution is expected to be about 100 ps (r.m.s.). Momentum resolution for decay pions is about 3×10^{-4} (r.m.s.)

All these parameters can be achieved by using the magnetic elements and the detector package of the HES magnetic spectrometer.

6.8 Expected Hypernuclear Yields

The forward produced kaons are a good trigger for hypernuclei production: about 3% of them are associated with "direct" and 10% with "indirect" production of hypernuclei. The remaining 87% of kaons are associated with "quasi-free" produced Λ particles, 64% of which decay through the $\Lambda \to \pi^- + p$ channel. The produced hypernuclei, besides light ($^{3}_{\Lambda}H$, $^{4}_{\Lambda}H$) ones, will stop in the target and decay after some 200ps with corresponding decay widths. The π^- decay widths for light hypernuclei ($A \le 12$) lie in the range 0.1-0.5 (Table 11), e. g. the π^- decay width of the $^{12}_{\Lambda}B$ hypernucleus, which is produced directly, through the $\gamma + {}^{12}C \to {}^{12}_{\Lambda}B + K^+$ reaction is expected to be 0.286 [13]. Therefore, the π^- decay rate of the $^{12}_{\Lambda}B$ from direct photoproduction, is expected to be: $R_{\pi^-}(^{12}_{\Lambda}B) = 0.03\times0.286\times R_K = 0.0086\times R_K$, where R_K is the kaon rate. For the "indirectly" produced hyperfragments, the corresponding π^- decay rates is determined as: $R^i_{\pi^-} = 0.1\times\varepsilon^i_{hyp}\times\Gamma^i_{\pi^-}\times R_K$, where ε^i_{hyp} and $\Gamma^i_{\pi^-}$ are population weights of hypernuclear isotopes and their π^- decay widths, respectively (see Table 11). The π^- decay rate from the "quasi-free" produced Λ particles is determined as: $R_{\pi^-}(\Lambda_{q.f.}) = 0.87\times0.64\times R_K \cong 0.56\times R_K$.

Taking into account direct and indirect production mechanisms we can estimate hyperfragment yields. We will consider the HKS experiment, a 30 μA electron beam, typical for HKS experiments and a ^{12}C target with an effective thickness of 100 mg/cm^2 or 5×10^{21} nuclei/cm^2 (24 mg/cm^2 ^{12}C foil tilted by about 10 degrees). The typical rate of the K^+ in HKS in these conditions is ~150 kaon/s. The survival rate of the 100 MeV/c pions in the $H\pi S$, with 4 m flight-path length is about 0.5. The total π^- rate detected in the $H\pi S$ in coincidence with HKS is:

$$R_{\pi^-}(H\pi S) = [\Delta\Omega/(4\times\pi)]\times\varepsilon_s\times[R_{\pi^-}(^{12}_{\Lambda}B) + \sum_i R^i_{\pi^-} + R_{\pi}(\Lambda_{q.f.})]\times R_K .$$

The hypernuclide and decay pion "daily" yields for 30 μA electron beam and 100 mg/cm^2 ^{12}C target are listed in Table 13. The "daily" yield of K^+ mesons, $N^K_{daily} = 150\times3600\times24 \equiv 1.3\times10^7$. For $^{12}_{\Lambda}B$ we consider only direct production mechanism. In Table 13 the renormalized relative weights and the decay pion yield from quasi-free produced Λ is listed as well. The momentum interval of pions from "quasi-free" produced Λ is about 100 MeV/c. Therefore in the $\Delta p = 100$ keV/c momentum interval, the "daily" yield from "quasi-free" produced Λ is about 8.6 and will be minimized essentially by using "vertex cat". The expected discrete pion spectra detected in $H\pi S$ are sown in Fig. 17.

Table 13: Hypernuclide and decay pion "daily" yields for 30 μA electron beam and 100 mg/cm^2 ^{12}C target.

Hypernuclide	Relative weight	Hypernuclide "daily" yield	π^--decay width: $\Gamma_{\pi^-}/\Gamma_\Lambda$	Decay π^-	Decay π^- detected in $H\pi S$
q. f. Λ	0.87	1.13×10^7	0.64	0.72×10^7	8.6×10^3
$^3_\Lambda H$	0.005	6.5×10^4	0.3	1.95×10^4	23
$^4_\Lambda H$	0.004	5.2×10^4	0.5	2.6×10^4	31
$^5_\Lambda He$	0.045	58.5×10^4	0.34	19.9×10^4	239
$^7_\Lambda Li$	0.0056	7.3×10^4	0.304	2.2×10^4	27
$^8_\Lambda Li$	0.0197	25.6×10^4	0.368	9.4×10^4	113
$^8_\Lambda Be$	0.0017	2.2×10^4	0.149	0.33×10^4	4
$^9_\Lambda Be$	0.0055	7.15×10^4	0.172	1.2×10^4	15
$^{11}_\Lambda B$	0.0018	2.3×10^4	0.213	0.49×10^4	6
$^{12}_\Lambda B$	0.03	11.2×10^4	0.286	11.1×10^4	134

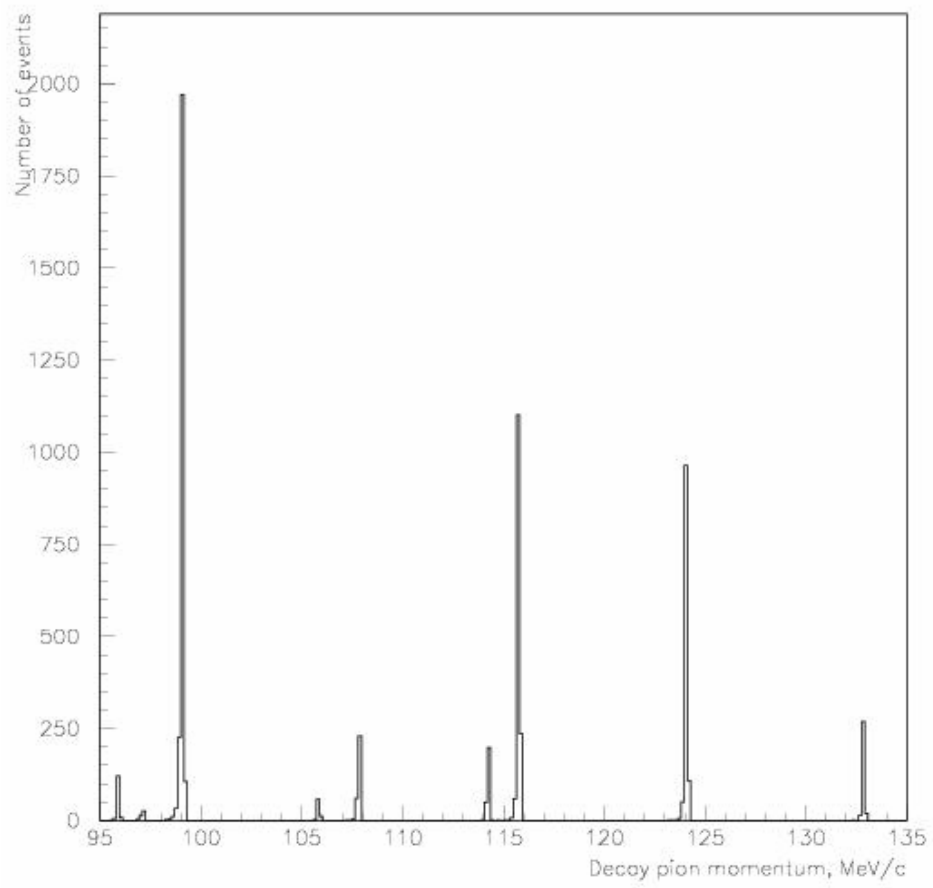

Figure 17: Expected π^- decay spectra from different hyperfragments with their relative weights; the dE/dx are taken into account; target thickness is 24 mg/cm^2. The $H\pi S$ resolution $\sigma = 3\times10^{-4}$; number of events is 6000, which is equivalent of 10 day 30 μA electron beam time.

6.9 Background

In the real experimental conditions the monochromatic pion spectra will be masked by a huge amount of background. We have three sources of background:

a) The promptly produced pions;
b) The decay pions from "quasi-free" produced Λ particles;
c) Accidentals.

The promptly produced pions will be excluded by using coincidence with produced kaons. However these ways don't allow excluding background from the decay of "quasi-free" produced Λ particles or from accidentals. We carried out simulation studies of the decay pion spectra from "quasi-free" produced Λ particles by using the Monte Carlo method. We take into account the following factors for the final distribution:

1. The momentum distribution of the "quasi-free" produced Λ particles. We assume isotropic production with Gaussian distribution (mean value is 200 MeV/c, $\sigma = 100\,\text{MeV/c}$).
2. The full π^- spectra are: 93.5% pions from "quasi-free" produced Λ particles, and 6.5% monochromatic pions from different hyperfragments with their relative weights, evaluated from the last column of Table 13.
3. The momentum resolution of the pion spectrometer.
4. The ionization energy loss.

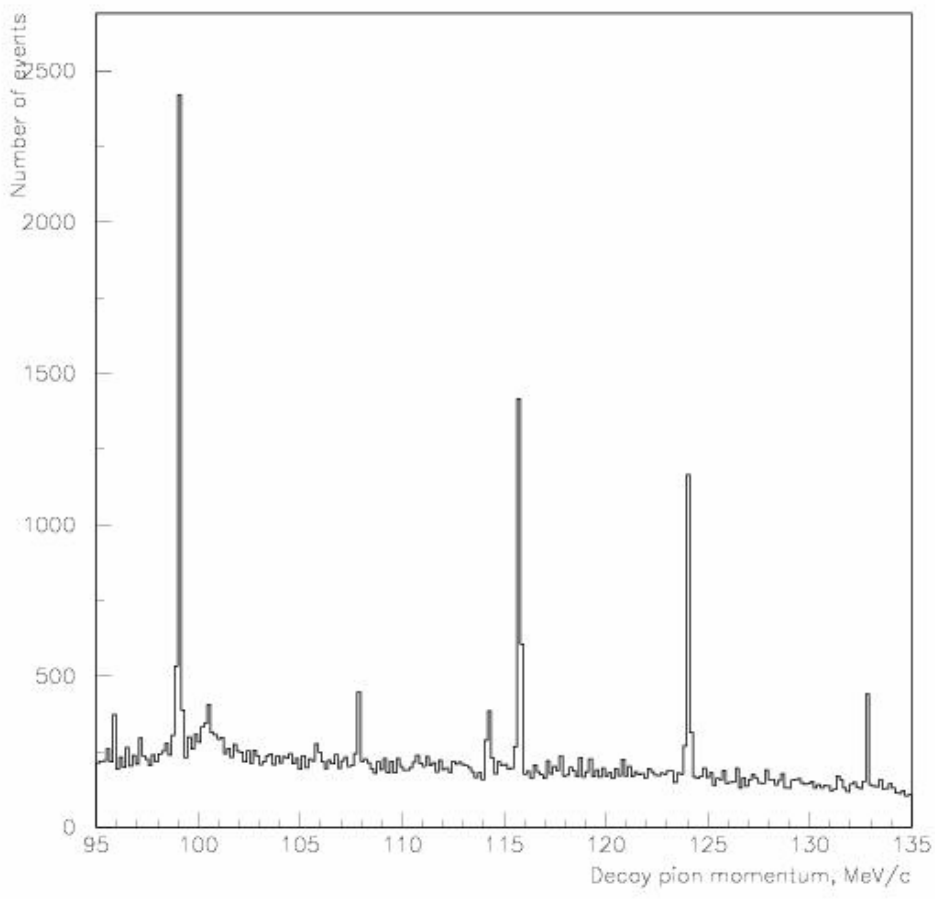

Figure 18: Simulated spectrum of the decayed pions (93.5% from quasi-free produced Λ particles, and 6.5% from different hyperfragments with their relative weights). Target thickness is 24 mg/cm^2; momentum resolution of $H\pi S$ is: $\sigma = 3\times10^{-4}$, total number of events is 10^5.

The simulated spectra with total of 10^5 pions produced in the 24 mg/cm^2 carbon target and measured in the $H\pi S$ with precision $\sigma = 3\times10^{-4}$ are shown in Fig. 18. These results demonstrate

that monochromatic pion spectra are clearly seen among a huge amount of quasi-free background, even without "vertex cut".

The "quasi-free" background can be suppressed additionally by using a "vertex cut", which requires the reaction point and the decay point to be in coincidence at a three-dimensional point. The simulated momentum and flight distance distribution of "quasi-free" produced Λ particles are shown in Fig. 19. For the Λ particle a lifetime of 228 ps was used. At JLab the reaction point can be determined with a precision better than 1 mm by using beam raster information (original size of the beam is about $\sigma \cong 150\,\mu m$). The "quasi-free" background practically can be eliminated if the decay point could be reconstructed with a precision of about 1 mm by using $H\pi S$ tracking information.

.

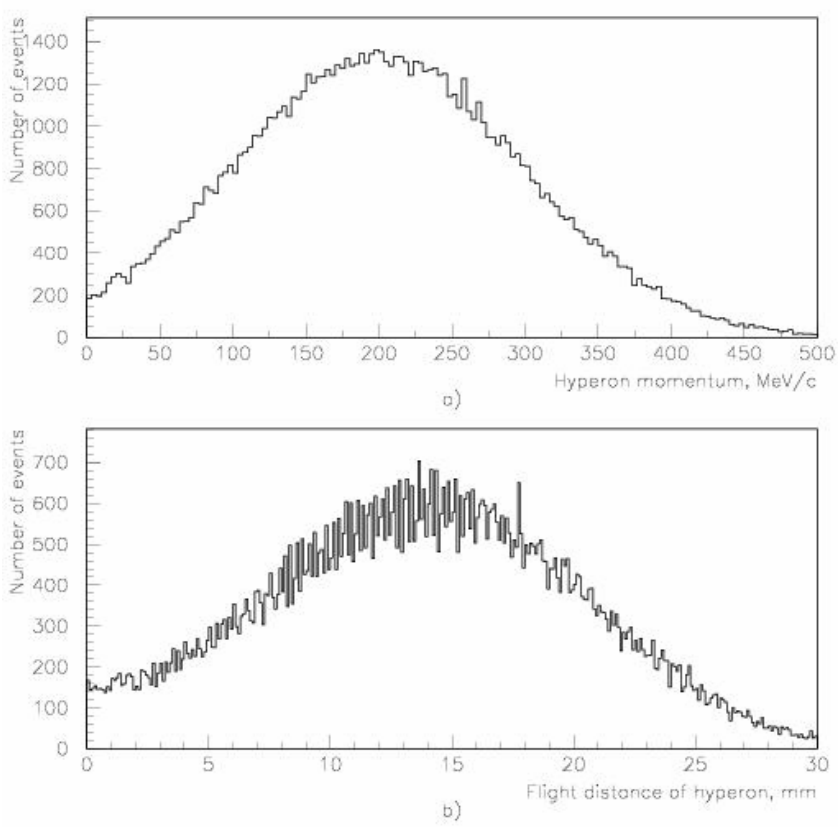

Figure 19: Simulated momentum (a) and flight distance (b) distributions of the "quasi free" produced Λ particles. For the lifetime of Λ particles 263 ps was taken.

6.10 Accidentals

The typical rate of kaons detected in the HKS is about 200 count/s (with 30 μA beam current and a 100 mg/cm^2 C target). The simulations from the Radiation Control group (Pavel Degtiarenko) for a 30% momentum acceptance and 30 msr solid angle for the pion spectrometer show a 1.4×10^3/sec negatively charged pion rate. This implies an accidental rate of 5.6×10^{-4}/sec within a 2 ns time window. In the 100 keV/c momentum bites in which the discrete pions are localized, this rate will be about 2×10^{-6}, which is negligible.

6.11 Requested Beam Time

In the *First Step* we intend to measure precisely the decay pion spectra of light hypernuclei which are produced in electron nuclear interactions "directly" or "indirectly". Our main goal is to measure precisely the binding energies, at least of ${}^{3}_{\Lambda}H$, ${}^{4}_{\Lambda}H$, ${}^{12}_{\Lambda}B$ hypernuclides and other hyperfragments which will show up in $H\pi S$. Therefore, we propose to use three production

targets: ^{12}C, ^{7}Li and ^{4}He. It is expected that by decreasing the target mass number, the production rates of $^{3}_{\Lambda}H$ and $^{4}_{\Lambda}H$ are increased.

It is worthwhile to note that the expected spectra will be more complicated than the spectra presented in Fig. 19 (due to existence of three body decays, different initial and final states in the two body decays, etc. [13]). We ask 10 day beam time for each target for the *First Step* experiment. The requested data taking hours were calculated so that at least about 500 counts for $^{3}_{\Lambda}H$ and $^{4}_{\Lambda}H$ can be accumulated.

The experience gained in these investigations will be used for planning the *Next Step* program.

7. Next Step: $H\pi S$ + new Detector Package based on the RF Cherenkov Timing Technique

7.1 Experimental setup and expected performance

The experimental setup in this case is basically different than in the case of *First Step***.** It consists only with the decay pion spectrometer $H\pi S$.

7.2 Detector package of the $H\pi S$

The tracking detector package of the *Next Step* decay pion spectrometer is the same as in the *First Step* decay pion spectrometer, but as a time-of-flight technique, we propose to use a new RF Cherenkov picosecond timing technique.

7.3 RF Cherenkov picosecond timing technique

A new particle identification device for $H\pi S$ is proposed. It is based on the measurement of time information by means of a new radio frequency picosecond phototube (RFPP) and time measuring concept. The technique is described in another LOI presented to this PAC [4].

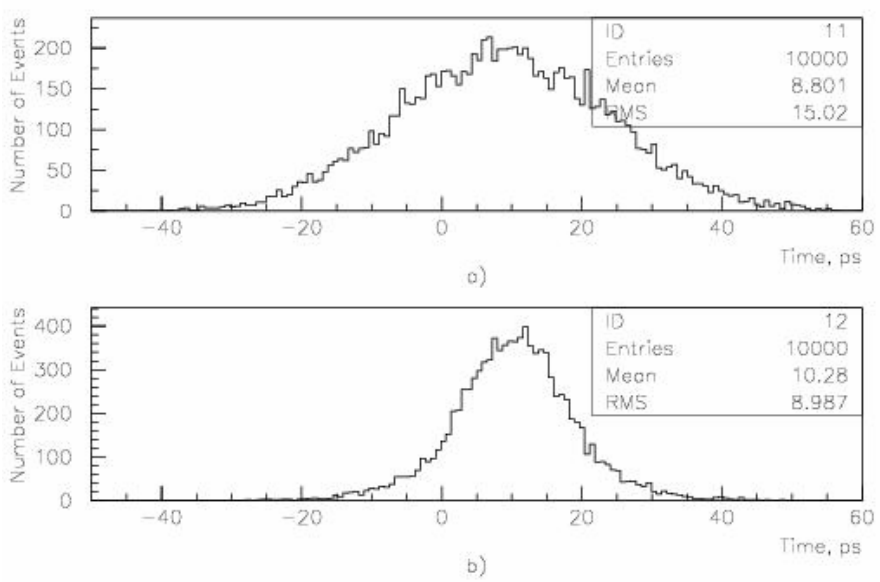

Figure 20: Simulated TOP distribution for the RF TOF Cherenkov detector of single photoelectrons (a) and mean TOP distribution of all detected photons (b).

The simulated time of propagation (TOP) distribution of single photoelectrons and mean TOP distribution of all detected photons- N_0 ($N_0 = 90 \times \langle \sin^2 \theta_c \rangle \, \mathrm{cm}^{-1}$, where θ_c is a Cherenkov photon emission angle [38]), for a head-on Cherenkov time-of-flight (TOF) detector with RFPP (time resolution σ = 15 ps) and with 2mm thickness Cherenkov radiator (refractive index n = 1.82), and for tracks of p = 115 MeV/c pions, are shown in Fig. 20a and 20b respectively. So the expected time resolution of the new Cherenkov timing technique is about 20 ps FWHM. The expected

reconstructed production or decay time precision for pions in $H\pi S$ is about or less than 30 ps FWHM, if the pion's transit time in $H\pi S$ is determined with precision better than 20 ps, FWHM.

7.4 Delayed π^- spectroscopy

In this case decay pions are separated from the huge amount of promptly produced background by using time information of the RF Cherenkov timing technique and reconstructing decay time by using tracking information of the $H\pi S$. This is possible at JLab because promptly produced pions have the same time structure as the incident electron beam (1.67 ps each 2ns) and the production times can be reconstructed with 30 ps (FWHM) precision. The reconstructed time distributions for prompt and decayed pions are shown in Fig. 21[a,b].

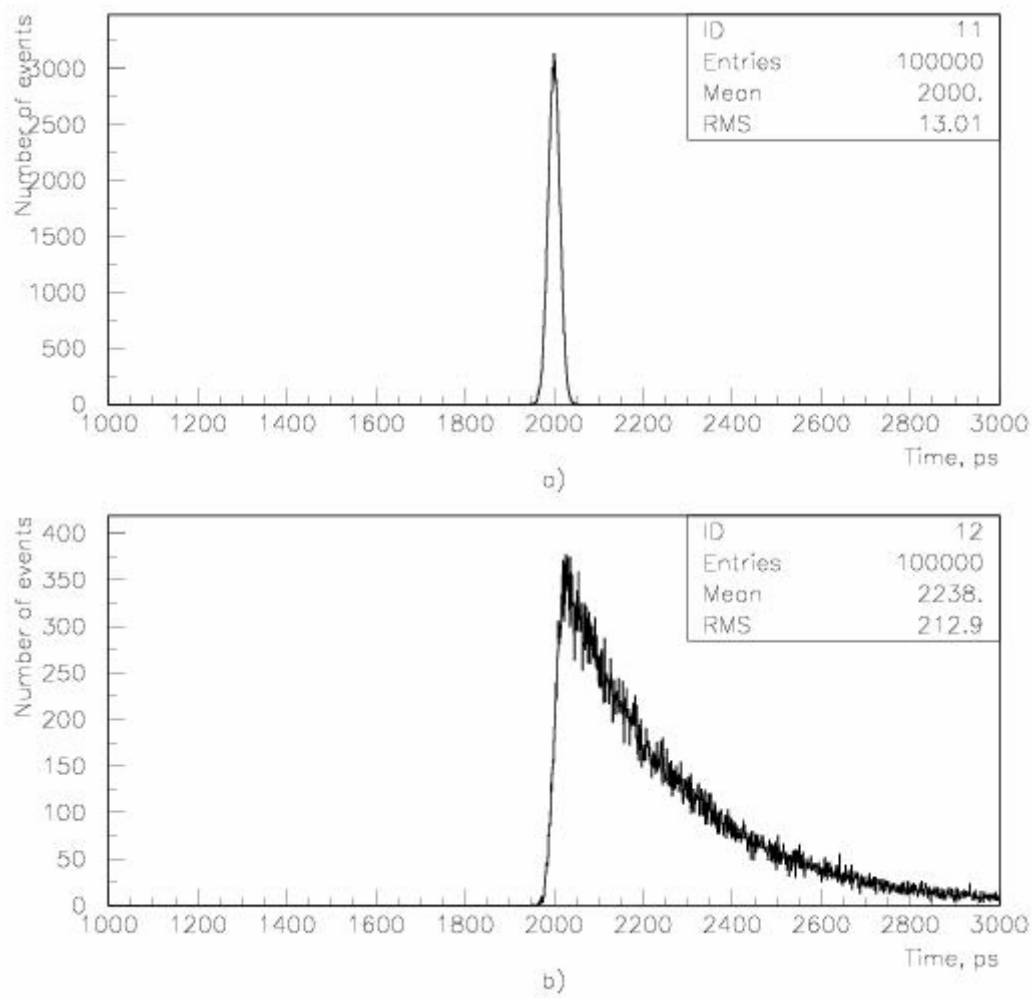

Figure 21: Reconstructed time distributions. (a) prompt pion, (b) delayed pion (lifetime = 260 ps). Total time resolution = 30 ps FWHM.

It follows from Fig 21[a,b] that the probability to find promptly produced pions in the region with times larger than 100 ps is less than 10^{-5} and that ~70% of decay pions from Λ or hyperfragments (lifetime 260 ps), have times larger than 100 ps. However in this way we can eliminate only promptly produced pions. Delayed pions from quasi-free produced Λ particles can be suppressed by using a "vertex cut". Therefore, the $H\pi S$ and RF Cherenkov timing technique with the JLab electron beam allows separate hyperfragment decay pions from promptly produced pions and from Λ-decayed pions, by using reconstructed time, reconstructed "vertex", and the interaction point of electron beam with target.

7.5 Yield estimation and comparison with other facilities in the world

Taking into account direct and indirect production mechanisms we can estimate hyperfragment yields. We will consider a 2 GeV electron beam (virtual photon flux in the 1-2 GeV energy range) and a ^{12}C target with an effective thickness of 100 mg/cm^2 or 5×10^{21} nuclei/cm^2 (24 mg/cm^2 ^{12}C foil tilted by about 10 degrees). The virtual photon flux is estimated to be $0.015\times N_e\times dE_\gamma / E_\gamma$ [39]. This gives about 1.35×10^{12} photon/sec for the 30 μA electron beam typical for HKS experiments. The $\gamma+^{12}C\rightarrow^{12}_{\Lambda}B+K^+$ reaction cross sections in the energy range 1-2 GeV is about 30 nb and expected $^{12}_{\Lambda}B$ hypernuclide and decay pion "daily" yields for a 30 μA electron beam, 100 mg/cm^2 ^{12}C target, and for the case of $H\pi S$ operation alone are summarized in Table 14. Here we use the direct production cross section. In addition the decay pion rate from background quasi-free produced Λ particles is listed in Table 14. In this case (without coincidence with kaons) the decay pion rate from quasi-free Λ particles is about the same order or higher than the expected discrete decay pion rates.

Table 14: Hypernuclide and decay pion "daily" yields for 30 μA electron beam and 100 mg/cm^2 ^{12}C target.

Hypernuclide	$^{12}_{\Lambda}B$
Photo production cross section in μb	0.03
Produced $^{12}_{\Lambda}B$	1.8×10^7
Decay pion width ($\Gamma_{\pi^-}/\Gamma_\Lambda$)	0.286
Decay pions from $^{12}_{\Lambda}B\rightarrow^{12}C+\pi^-$	4.9×10^6
Decay pions from $^{12}_{\Lambda}B\rightarrow^{12}C+\pi^-$, detected in $H\pi S$	6×10^3
Decay pions detected in $H\pi S$ in coincidence with HKS (150 kaon/sec)	134
Prompt pions detected in $H\pi S$ (Δp = 100 keV/c)	4.1×10^5
Decay pions from q. f. produced Λ detected in $H\pi S$ (Δp = 100 keV/c)	8.9×10^3
Decay pion momentum (MeV/c)	115.8

For the hyperfragments, that is of hypernuclei with a mass number lower than the production target one, the expected rates are much higher. Table 15 reports a comparison between the expected hyperfragment yields at JLab and at DAΦNE2 and J-PARC. The total decay pion rate from all produced hyperfragments was estimated by using average $\Gamma_{\pi^-}/\Gamma_\Lambda = 0.3$.

Table 15: Comparison between the expected hyperfragment "daily" yields at JLab (30 μA electron beam and 100 mg/cm^2 ^{12}C target) and at DAΦNE2 and J-PARC K1.1 line. (For the latter cases numbers are taken from Ref. [40].)

Accelerator	JLab	DAΦNE2	J-PARC
Stopped K^-		1.26×10^9	1.33×10^8
Produced strangeness	1.28×10^{10}	1.26×10^9	1.33×10^8
Hyperfragment formation probability	0.1	0.1	0.1
Produced hyperfragments	1.28×10^9	1.26×10^8	1.33×10^7
Decay pions from hyperfragments	3.84×10^8		
Decay pions from hyperfragments detected in $H\pi S$	3.2×10^5		

Therefore the production of hypernuclei and hyperfragments with the JLab electron beam and detection of their decay pions by using the high resolution magnetic spectrometer and the high precision timing technique is a very encouraging perspective for investigating hypernuclei. This will be the most precise and sensitive decay pion spectroscopy possible in the near future.

8. Summary

High resolution decay pion spectroscopy for light targets has been proposed.

The present proposal postulates two stages for the proposed experimental program. The first stage postulates that we use the high resolution kaon spectrometer (HKS) and high resolution pion spectrometer ($H\pi S$), e. g. a modified version of HES. In this stage we propose to use the existing detector packages of HKS and HES and carry out decay pion spectroscopy for the three light targets ${}^{4}He$, ${}^{7}Li$, and ${}^{12}C$, and measure precisely binding energies of produced light hypernuclei or hyperfragments. The proposal is based on the success of the operation of these magnetic spectrometers in Hall C at JLab and will fully explore taking advantage of the lab's high-quality high-power CW electron beams.

Meanwhile, the high-resolution RF Cherenkov picosecond timing technique has been proposed for simultaneous development.

The next step postulates that we use the high resolution pion spectrometer ($H\pi S$) and high resolution RF Cherenkov timing technique as a highly sensitive decay pion spectrometer. Once the first step of the proposed experiment is successfully performed and the Cherenkov picosecond timing technique is developed, the next stage of hypernuclear physics program by the decay pion spectroscopy will be fully explored, taking advantage of the new timing technique and JLab's RF driven CW electron beams with fine time structure as highly sensitive and high resolution decay pion spectroscopy of Λ hypernuclei. The fine time structure of the RF driven CW electron beams at JLab (1.67 ps duration bunches each 2 ns) is very suitable for applying the $H\pi S$ with RF Cherenkov picosecond timing technique for hypernuclear studies, considering discrete pion decay of hypernuclides with lifetimes of about 200 ps as a "delayed-particle spectroscopy", similar to "delayed γ-ray spectroscopy" in nuclear spectroscopy.

The physics subjects which can be investigated by means of decay pion spectroscopy include: (1) YN interactions, (2) study of exotic hypernuclei, (3) impurity nuclear physics, and (4) medium effect of baryons. This will be the most sensitive experiment for the detecting of exotic hypernuclides with extreme neutron and proton numbers, with about 3.2×10^{5} detected hyperfragment "daily" yield. For comparison let us note that the total emulsion data on π^{-}-mesonic decays amount to some 3.6×10^{4} events from which of about 4000 events are identified.

High momentum resolution and high time resolution of the $H\pi S$ with the RF Cherenkov picosecond technique are very suitable especially for investigation of impurity nuclear physics and medium effects of baryons at JLab by using the "tagged weak π^{-} decay method".

The proposed experiment is a unique one and is not duplicated by any in the currently approved or planned experimental program.

References

1. D. H. Davis, "50 years of hypernuclear physics, I. The early experiments", Nucl. Phys. A 754 (2005) 3c.
2. R. H. Dalitz, "50 years of hypernuclear physics, II. The later years", Nucl. Phys. A 754 (2005) 14c.
3. G. Keyes, M. Derrick, T. Fields et al., "Properties of the hypertriton", Phys. Rev. D1, 66 (1970).
4. A. Margaryan, O. Hashimoto, S. Majewski, L. Tang "RF Cherenkov picosecond timing technique for Jlab 12 GeV physics program" LOI to this PAC.
5. O. Hashimoto, L. Tang, J. Reinhold (spokespersons), "Spectroscopic study of Λ hypernuclei up to medium-heavy mass region through the in the (e, e'K^+) reaction", JLAB Experiment E01-011.
6. O. Hashimoto, S. Nakamura, L. Tang, J. Reinhold "Spectroscopic investigation of Λ hypernuclei in the wide mass region using the (e, e'K^+) reaction", JLAB Experiment E05-115.
7. J-PARC Strangeness Nuclear Physics Group, Letter of intent for "New generation spectroscopy of hadron many body systems with strangeness S=-2 and -1", Letter of intent for nuclear and particle physics experiments at the J-PARC, J-PARC 03-6.
8. O. Hashimoto, H. Tamura, "Spectroscopy of Λ hypernuclei", Progress in Particle and Nuclear Physics 57 (2006) 564-653.
9. Th. Rijken, Y. Yamamoto, "Recent soft-core baryon-baryon interactions", Nucl. Phys. A 754 (2005) 27c.
10. A. Nogga, "Faddeev-Yakubovski calculations for A=4 hypernuclear system", Nucl. Phys. A 754 (2005) 36c.
11. Y. Fujimura, C. Nakamoto, M. Kohno, Y. Suzuki, K. Miyagawa, "Interactions between octet baryons and their applications to light hypernuclei", Nucl. Phys. A 754 (2005) 43c.
12. H. Nemura, Y. Akaishi, and Y. Suzuki, "Ab initio Approach to s-Shell Hypernuclei ${}^{3}_{\Lambda}H, {}^{4}_{\Lambda}H, {}^{4}_{\Lambda}He, and\ {}^{5}_{\Lambda}He$ with a $\Lambda N - \Sigma N$ Interaction", Phys. Rev. Lett. 89 (2002) 142504-1.
13. T. Motoba and K. Itonaga, "Pi-Mesonic Weak Decay Rates of Light-to-Heavy Hypernuclei", Progress of Theoretical Physics Supplement, No. 117, (1994) p.477.
14. T. Motoba, "Mesonic weak decay of strange nuclear systems", Proceedings of the IV International Symposium on Weak and Electromagnetic Interactions in Nuclei, 12-16 June 1995, Osaka, Japan. Edited by H. Ejiri, T. Kishimoto and T. Sato, World Scientific, 1995, p.504.
15. E. Hiyama, M. Kamimura, T. Motoba, T. Yamada, Y. Yamamoto, "Three-body model study of $A = 6 - 7$ hypernuclei: Halo and skin structures", Phys. Rev. C53, (1996) 2075.
16. L. Majling et al., "Superheavy Hydrogen Hypernucleus ${}^{6}_{\Lambda}H$ ", AIP Conference Proceedings Volume 831, (2006)p. 493.
17. P. K. Saha, T. Fukuda and H. Noumi, "Neutron-reach hypernuclei by the double-charge exchange reaction", Letter of Intent for Nuclear and Particle Physics experiments at the J-PARC (LOI9), 2002.
18. E. Hiyama, M. Kamimura, K. Miyazaki, T. Motoba, "γ-transitions in A=7 hypernuclei and a possible derivation of hypernuclear size", Phys. Rev. C59 (1999)2351.
19. K. Tanida, H. Tamura, D. Abe et al., "Measurement ob the B(E2) of ${}^{7}_{\Lambda}Li$ and Shrinkage of the Hypernuclear Size" Phys. Rev. Lett. 86 (2001) 1982.
20. H. Tamura, "High resolution spectroscopy of Λ hypernuclei: present status and perspectives", Nucl. Phys. A691 (2001) 86c. "Impurity nuclear physics: Hypernuclear γ spectroscopy and future plans for neutron-reach hypernuclei" The European Physical Journal A-Hadrons and Nuclei, V13 (2002) 181.
21. R. H. Dalitz and A. Gal "The formation of, and the γ-radiation from, the shell hypernuclei" Ann. Phys. 116 (1978) 167.
22. D. J. Millener, "Shell-model description of Λ hypernuclei", Nucl. Phys. A691 (2001) 93c.
23. M. Juric, G. Bohm, J. Klabuhn et al., "A new determination of the binding-energy values of the light hypernuclei (A≤ 15)", Nucl. Phys. B 52 (1973) 1.

24. T. Yamazaki et al., “New aspects and new tools in hypernuclear studies: experiments with a superconducting toroidal spectrometer” INS-Rep.-728 (1988).
25. H. Outa et al., “Lifetime measurement of ${}^{4}_{\Lambda}H$ hypernucleus”, INS-Rep.-914 (1992).
26. The FINUDA Collaboration, “FINUDA A DETECTOR FOR NUCLEAR PHYSICS AT DAΦNE, LNF-93/021 (1993).
27. F. X. Lee, T. Mart, C. Bennhold, H. Haberzettl, L. E. Wright, ”Quasifree Kaon Photoproduction on Nuclei”, arXiv: nucl-th/9907119.
28. H. Yamazaki et al., “The ^{12}C(γ, K^{+}) reaction in the threshold region”, Phys. Rev. C 52, R1157–R1160 (1995).
29. M. Sotona et al., Proceedings of Mesons and Light Nuclei ’98, (1998) 207.
30. T. Mart, D. Kusno, C. Bennhold, L. Tiator, D. Drechsel, “Photoproduction of the hypertriton”, arXiv: nucl-th/9610038.
31. T. Mart, L. Tiator, D. Drechsel, C. Bennhold, “Electromagnetic production of the hypertriton”, arXiv: nucl-th/9708012, Nucl. Phys. A640 (1998) 235.
32. F. Dohman et al., “Angular distributions for hyper He-3 He-4 bound states in the He-3 He-4(e, e-prime K+) reaction, Phys. Rev. Lett. V 93 (2004) 242501.
33. H. Tamura, T. Yamazaki, R. S. Hayano et al., “Formation of ${}^{4}_{\Lambda}H$ hypernuclei from K^{-} absorption at rest on light nuclei”, Phys. Rev. C 40 (1989) R479.
34. H. Tamura, T. Yamazaki, M. Sano et al., “Compound-hypernucleus interpretation on ${}^{4}_{\Lambda}H$ formation probabilities in stopped- K^{-} absorption”, Phys. Rev. C 40 (1989) R483.
35. Y. Nara, A. Ohnishi and T. Harada, “Target mass dependence of ${}^{4}_{\Lambda}H$ formation mechanism from K^{-} absorption at rest”, *Phys. Lett.* 346 *(1995)* 217.
36. Lubomir Majling, “Hypernuclei ${}^{4}_{\Lambda}H$ and ${}^{6}_{\Lambda}H$ could be identified – so what?”, IX International Conference on Hypernuclear and Strange Particle Physics, October 10-14, 2006, Mainz, Germany.
37. K. A. Ispirian, A. T. Margarian, A. M. Zverev “A Monte Carlo method for calculation of the distribution of ionization losses”**,** Nucl. Instr. and Meth.117 (1974) 125.
38. Particle Data Group, Phys. Rev. D. 50 (1994) 1261.
39. Yung-Su Tsai, “Pair production and bremsstrahlung of charged leptons”, Rev. of Mod. Phys., 46 (1974) 815.
40. T. Bressani et al., “Hypernuclear physics at DAΦNE2”, Nucl. Phys. A 754 (2005) 410c.